

An engineering guide to superconducting quantum circuit shielding

Elizaveta I. Malevannaya,^{1,2} Viktor I. Polozov,¹ Anton I. Ivanov,^{1,2} Aleksei R. Matanin,¹ Nikita S. Smirnov,¹ Vladimir V. Echeistov,¹ Dmitry O. Moskalev,¹ Dmitry A. Mikhailin,¹ Denis E. Shirokov,¹ Yuri V. Panfilov,¹ Ilya A. Ryzhikov,^{1,3} Aleksander V. Andriyash,² and Ilya A. Rodionov^{1,2}

¹⁾*Shukhov Labs, Quantum Park, Bauman Moscow State Technical University, Moscow, 105005, Russia*

²⁾*Dukhov Automatics Research Institute, VNIIA, Moscow, 127055, Russia*

³⁾*Institute of Theoretical and Applied Electrodynamics, Moscow, 125412, Russia*

(*Electronic mail: irodionov@bmstu.ru)

(Dated: 16 June 2025)

In this review, we provide a practical guide on protection of superconducting quantum circuits from broadband electromagnetic and infrared-radiation noise by using cryogenic shielding and filtering of microwave lines. Recently, superconducting multi-qubit processors demonstrated quantum supremacy and quantum error correction below the surface code threshold. However, the decoherence-induced loss of quantum information still remains a challenge for 100+ qubit quantum computing. Here, we review the key aspects of superconducting quantum circuits protection from stray electromagnetic fields and infrared radiation – multilayer shielding design, materials, filtering of the fridge lines and attenuation, cryogenic setup configurations, and methods for shielding efficiency evaluation developed over the last 10 years. In summary, we make recommendations for creation of an efficient and compact shielding system as well as microwave filtering for a large-scale superconducting quantum systems.

I. INTRODUCTION

One of the most promising physical realizations of quantum computers and simulators are superconducting quantum circuits (SQC)^{1–4}. Nowadays, there are several superconducting quantum computer prototypes capable to solve very complex specific tasks, which are not amenable for the state-of-the-art supercomputers^{5–9}. However, quantum information loss or decoherence is still one of the key challenges on the way to the useful quantum computers. Robust error-free operation of the superconducting qubits, which are extremely sensitive to noise^{10–14}, requires minimizing both external and internal sources of noise. Internal sources can be combated by improving the design^{15,16}, materials^{17–19} and technology^{20,21} of quantum circuits.

In the last two decades, the leading scientific groups in the field demonstrated tremendous results in minimizing the internal noise sources including magnetic vortices²², quasiparticle tunneling^{23–25}, two-level systems^{22,24} and dielectric losses in substrate^{26–28}. A number of papers are devoted to an external noise sources suppression, such as flux and charge noise²², Purcell effect²⁹, interaction with stray electromagnetic modes of a cryogenic experimental setup or environment^{23,24}. However, superconducting circuits protection from a broadband spontaneous radiation: from surrounding equipment (frequency below 300 GHz, wave length more 1 mm), infrared (IR) radiation (frequency from 300 GHz to 430 THz, wave length from 0.74 μm to 1 mm), cosmic rays, and background radiation (frequency above 430 THz, wave length less 0.74 μm)^{23,30} is currently being researched.

To satisfy the $kT \ll \hbar\omega$ condition³¹ the superconducting qubits operating in GHz frequency range, should be placed at near absolute zero temperature (in dilution refrigerators (or fridges) below 50 mK). Within the fridge, there are several sources of infrared radiation³². First, there are warmer stages of the fridge itself, and second, the passive elements of the

cryogenic setup, which can dissipate electrical energy as a heat. An important factor of the decoherence is an interaction of SQC with an infrared (IR) radiation. The power transferred to SQC from IR photons is greater than from cosmic rays or background radiation³³. At the same time, cosmic rays and background radiation have a greater penetrating power compared to IR radiation. We briefly discuss the protection from cosmic rays and background radiation below, but this work is mostly focused on protecting against electromagnetic fields and IR radiation, which are the main sources of external sources of decoherence.

External radiation may destroy Cooper pairs, generating quasiparticles, which then tunnel through a Josephson junction, which in turn results in both qubit energy relaxation and dephasing^{33–35}. An external magnetic field variation and induced charges near the Josephson junction area cause uncontrolled changes in the Hamiltonian parameters, specifically, the Josephson energy, E_J , the superconducting phase difference, δ , and the qubit frequency, ω_{01} ²². Thus, we especially focus on protecting superconducting quantum circuits from broadband external electromagnetic fields and IR-radiation. A spontaneous radiation can either be from a free space or coaxial microwave (MW) transmission lines installed in the fridge. Depending on the path of stray radiation propagation, i.e. in a free space or by microwave lines, various shielding systems or filtering are used. The most effective shielding can be achieved by combining these two approaches. The shielding of the SQC usually represents a system of nested cylinders surrounding the sample holder with a chip. We refer the metal enclosure embedding printed circuit board with a superconducting circuit as a sample holder.

Articles by leading scientific groups show a wide variety of shielding systems, which differ greatly in the number of shields and their combination^{18,36–43}. Comparing represented shielding systems, it can be seen that they differ from each other by the number of shields, their relative position, posi-

tion inside the dilution refrigerator, and the design and materials used.

Despite of the differences between considered shielding systems, there are also some common solutions:

1. Multilayered shielding. In considered works we found a trend towards gradual increase of the shielding complexity by adding of more shielding layers. In the papers over the last 5 years, three to six shields are used in the shielding systems. However, a single-layer shielding is still frequently used, and two-layer systems comprise the majority of all shielding configurations.
2. Versatility of shielding. Considered shielding systems consist of shielding layers protecting from both IR radiation and the magnetic field. Additionally, in some cases a single shield can combine the functions of IR and magnetic shielding. For this purpose, an IR-absorbent coating is applied to either a superconducting or magnetic metal shield.
3. IR shielding implementation. IR shielding is composed of a metal base with a specialized IR-absorbing coating based on the epoxy resin or mixture of epoxy resin and silicon carbide particles or graphite powder. This coating should exhibit a low level of reflectivity (up to 0.0001), i.e., high IR absorption.
4. Magnetic shielding implementation. Magnetic shielding consists of superconducting shields or shields made of metals with a high level of relative magnetic permeability (typically, more than 100,000).
5. In addition to the shields, various types of filters (including IR filters) protecting from an IR radiation are used.

At the same time the following problems can be highlighted after review of shielding system configurations:

1. There are no special guidelines for ordering the shields, recommendations for the shields' placement inside the dilution refrigerator, instructions to choosing a number of shields.
2. The absence of a clearly defined set of materials for the shields. Among the various materials used for shielding, the most commonly used can be identified, but there are no special instructions for their use.
3. There is no straightforward solution to the choice of sample holder's material and design.

Given the wide range of possible shielding configurations and materials, it is challenging to choose an optimal shielding system, which provides the highest level of protection, while maintaining simple design and fabrication.

The filtering systems are also varied from one scientific group to another. The filters are an integral part of the cryogenic setup for quantum systems. They are employed in all control and measurement lines of the fridge, specifically in readout, drive, and flux lines. There are many options of the filters

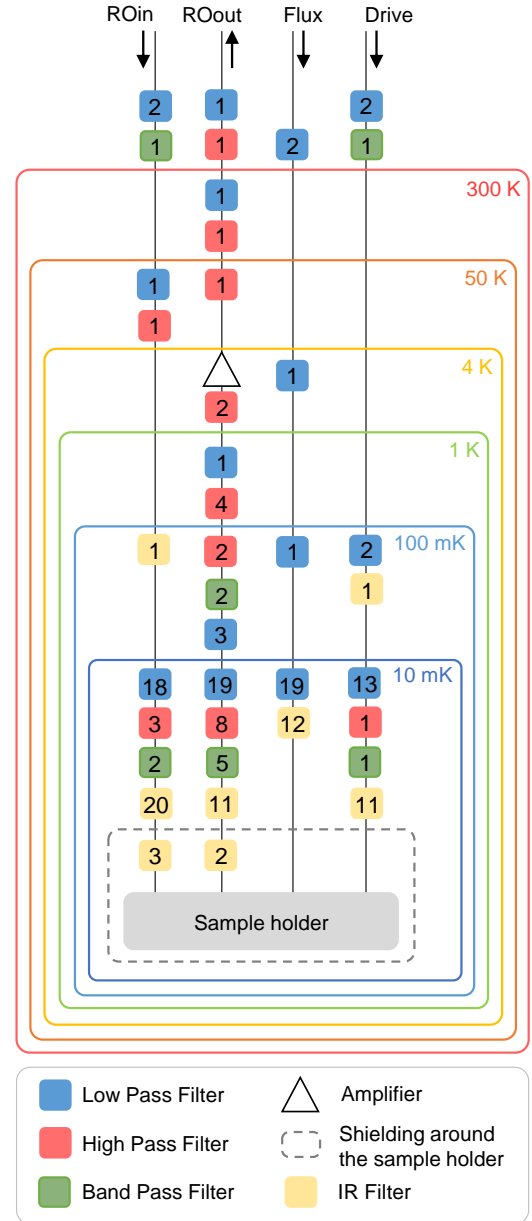


FIG. 1. Cryogenic setup with different filtering for MW and DC lines in a dilution refrigerator. The number on each element in setup represents the number of papers (from references list), which use the exact filter type at corresponding position.

placement in cryogenic measurement setup (see Fig. 1). In the same way as for the shielding systems, choosing the optimal filter position is also a challenging task.

This review represents set of requirements for choosing shielding and filtering system for effective protection of SQC from IR radiation and unwanted electromagnetic fields based on the analysis of existing multilayer shielding designs, used materials and signal lines filtering and attenuation.

A. Article organization

In the Section II, we discuss what type of shielding is required for protection from infrared radiation and stray electromagnetic fields. We present the requirements for an effective shielding system based on theoretical estimations and numerical modeling, and analyze existing shielding systems according to these requirements. We propose additional shielding techniques to improve protection efficiency, and demonstrate how the sample holder design affects the shielding effectiveness.

In Section III, we discuss microwave lines filtering. Specifically, we describe the requirements for the filters used in cryogenic setup for quantum systems. We explore the types of filters employed in measurement circuits and their placement in different measurement lines.

In Section IV, we discuss the methods for evaluating the effectiveness of shielding systems and compare different shields.

In summary and conclusions, we discuss the similarities and differences in the shielding of quantum circuits, and we also attempt presenting our recommendations for the compact and efficient quantum circuit protection against external electromagnetic fields.

II. SHIELDING

Generally, the shielding system solves two main problems: absorption of an incident IR radiation and protection from stray magnetic fields. In order to design an effective shielding system, it is essential to consider these problems individually: starting from shielding principles to the materials and designs used.

A. Protection from IR radiation

1. Shielding principle

Protection from an IR radiation is based on the absorption of the energy from incident photons by the absorbing material of a shield and the conversion of this energy into internal thermal energy of the shield. This thermal energy is then removed by the cooling mechanisms within the fridge. As a result, the photons partially or completely lose the energy and can't cause Cooper pairs braking in superconductor. To protect from the described source of an IR radiation, the shields and, in some cases, sample holder lids are coated by special IR absorbing materials. The absorption coefficient of such coatings can reach the value up to 0.9 in THz range of the electromagnetic spectrum⁴⁴. Commercially available epoxy resins, such as Stycast 2850 FT and Eccosorb CR series, are used as IR-absorbing coatings, either alone or in combination with other particles such as silicon carbide powder, carbon powder, or graphite dust.

2. Requirements for IR shielding

Based on the theory of heat transfer by radiation, the following concepts for an IR shielding can be formulated:

1. To improve IR radiation protection (see simulation below) and reduce weight we recommend the inner surface of the shield with an absorption coefficient close to 1 and the outer surface – approaching 0 (highly reflective) in order to reflect outside radiation.
2. Shield outer surface can be made of a smooth and polished metal to maximize reflection of outside IR radiation (minimal absorption coefficient).
3. The absorbing coating on the inner shield side should have an extended effective absorbing surface and high thermal conductivity for rapid heat dissipation.
4. In order to increase the absorption coatings capacity one should insure its surface roughness on the order of the IR wavelength⁴⁵. This level of roughness avoid specular reflection, scattering the incident IR radiation, which undergoes multiple reflections and corresponding interactions within absorption material, extending an effective surface and overall absorption. In cryogenic quantum applications a far-IR range with wavelengths of 700 – 1000 μm become one of the most important⁴⁶, consequently, macroscopic roughness of the same size should be introduced for better absorption capacity.
5. The temperature of the shield must be lower than the temperature of the quantum circuit to ensure the heat transfer from the sample to the shield. The shield base should be made of a metal with the highest possible thermal conductivity and have robust thermal contact between the shield and the lower stage of the fridge.

Following these requirements is the reliable way for creating an effective IR shielding. Let's consider the existing IR shields designs.

3. Practical implementation of IR shielding

a. Material for the IR shields base. Based on the requirements for IR shielding, it is necessary to use a shield base made of material with a high thermal conductivity. The thermal conductivity of some materials commonly used for the base of IR shields is represented in Table 1 below.

It can be clearly seen from Table 1, that high purity copper has a higher thermal conductivity, making it preferable material for the base of IR shielding.

The use of copper for the shielding base is also supported by shielding systems described the literature. Fig. 2 shows the most commonly used materials for the base of IR shielding described in^{38,49–52}. More than one-third⁵³ of all listed in Fig. 2 IR shields combine the IR and magnetic shielding. The base in these shielding systems is made of another materials, such

TABLE I. Thermal conductivity of materials used for IR shielding.

Material	κ , at 300 K, $W \cdot m^{-1} \cdot K^{-1}$	κ , at 4 K $W \cdot m^{-1} \cdot K^{-1}$
Copper (99.999%)	$\sim 400^{46}$	$\sim 15,000^{46}$
Gold	310^{47}	-
Aluminum (99.999%)	$\sim 400^{46}$	$\sim 3,000^{46}$
Brass	$\sim 150^{46}$	$\sim 4^{46}$
μ -metal	19^{48}	-

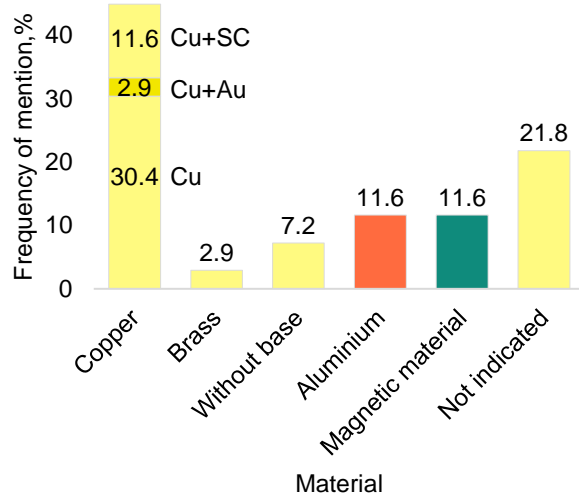


FIG. 2. Typical materials for the base of IR shields.

as copper coated with a superconductor^{39,54}, in particular superconducting aluminum^{55–57}, or μ -metal^{58,59}. The combination of IR and magnetic shielding allows for a more compact and lightweight shielding design. However, heat removal capabilities of these shielding systems are reduced compared to the system with a copper base.

Rarely, gold-plated copper^{60–62} is used as the base material for the IR shield. Gold-plating of the entire shielding components does not provide any advantages, as it reduces thermal conductivity at cryogenic temperatures compared to uncoated copper. However, gold-plating is highly beneficial for thermal interfaces between shielding components. Gold-gold contacts demonstrate over an order of magnitude greater thermal conductance than copper-copper contacts⁴⁶ due to the absence of surface oxidation and improved conformability⁶³. This enhancement relaxes the required surface finishing quality and contact pressure for copper interfaces.

b. Absorbing coating for IR shielding. Another important component of IR shielding is an IR absorbing coating. In reference⁶⁴, some absorbing coatings data, that are used in the IR radiation range, are provided (Eccosorb CR110, Herberts 1356H, TK RAM, and silicon carbide (SiC) grains in Stycast). Assuming that the IR shielding material does not transmit radiation, we can consider the sum of absorption and reflection coefficients to be 1. This allows us to estimate the absorption properties based on the reflection coefficient. Ac-

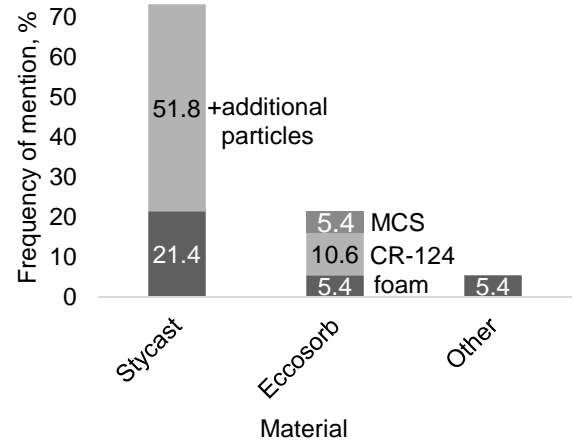


FIG. 3. Absorptive layer materials for an IR shielding.

cording to theory⁶⁵, absorbent coatings should exhibit maximum absorption (near 1) in the operating range. Among the absorbent coatings shown in reference⁶⁴, SiC grains in Stycast have the highest absorption capacity. For IR shielding, Stycast epoxy-based coatings are commonly used both in a pure form (references^{66,67}) and in combination with additional particles to enhance surface roughness (reference⁴⁴) (see Fig. 3). To form a relief of this surface, SiC particles of various sizes^{50,56,68} or carbon powder^{49,51,69} or thereof combination^{37,61}, can be used. The use of 1 mm size SiC particles mixed with Stycast epoxy is preferable due to its highest absorption capacity. Such particle size ensures the fulfillment of the surface roughness requirement for the IR range. Such particle size ensures the fulfillment of the surface roughness requirement for the IR range.

Other absorbent materials that may be used include epoxy resins and Eccosorb foams⁵⁹. Eccosorb CR-124^{23,70–72} and Eccosorb MCS in a paste form⁷³ are applied to the metal base. Eccosorb foam^{74–76} or MCS tape⁷⁷ may be wrapped directly around the sample holder. The thermal conductivity of these absorbent tapes and foams are on the order or less than $1 W \cdot m^{-1} \cdot K^{-1}$ ⁷⁸, that is much lower in comparison with metals thermal conductivity. At cryogenic temperatures the difference in thermal conductivity between Eccosorb and metals (base materials) increase due to the suppression of phonon thermal conductivity. For example, at around 1 K, the difference is already more than 5 orders of magnitude ($1000 W \cdot m^{-1} \cdot K^{-1}$ for oxygen-free copper compared to $0.0038 W \cdot m^{-1} \cdot K^{-1}$ for Eccosorb⁴⁶). With that in mind, it's recommended to use such absorbent materials in pair a high thermal conductivity metal base for better cooling efficiency.

c. Reflection layers. In addition to IR protection, thin metallic layers are used to reflect spontaneous parasitic IR radiation. For this purpose, metallic foils³⁸, films⁷⁴ or aluminized polyethylene terephthalate (trade name Mylar)^{18,55,75,79} may be used. The placement of this layer may vary: it may be placed around the holder¹⁸, around the first shield^{56,75}, between the shields^{39,55,56} or surround the entire shielding system^{18,39,56}. At the same time, the outer surface

of the shield may act as a reflective layer in case it has a low absorption coefficient. This allows for the creation of a more compact shielding system.

d. *The number of layers, the shape, and the arrangement of the IR shields.* A more effective shielding system can be defined using the theory of a heat transfer by radiation and modeling the radiation propagation in the "sample-shielding-dilution refrigerator" system. A calculation scheme is represented in Fig. 4. In this system, "Body 1" is the sample, "Body 2" is the dilution refrigerator or radiation source, and "Shields" is the shielding system, which effectiveness we'd like to estimate. The power of a heat transfer by radiation is calculated by the following relation:

$$Q_{(1,2)sh} = \sigma A_{(1,2)sh} F_1 (T_1^4 - T_2^4), \quad (1)$$

where σ is the Stefan-Boltzmann constant equal to $5.67 \cdot 10^{-8} \text{ W} \cdot \text{m}^{-2} \cdot \text{K}^{-4}$; F_1 is the surface area of Body 1; T_1 and T_2 are the temperatures of Bodies 1 and 2, respectively; and $A_{(1,2)sh}$ is the reduced absorption coefficient of the system (taking into account the shields): $A_{(1,2)sh} =$

$$\frac{1}{\frac{1}{A_{1,2}} + \sum_{i=1}^n \frac{F_1}{F_{shi}} \left(\frac{2}{A_{shi}} - 1 \right)};$$

where F_{shi} is surface area of i -th shield; A_{shi} is absorption coefficient of i -th shield; $A_{1,2}$ is reduced absorption coefficient between Body 1 and Body 2: $A_{1,2} = \frac{1}{\frac{1}{A_1} + \frac{F_1}{F_2} \left(\frac{1}{A_1} - 1 \right)}$;

where A_1 and A_2 are the absorption coefficients of Body 1 and Body 2, respectively; and F_2 is the surface area of Body 2.

In case the shield has different absorption coefficients of its inner and outer surfaces, formula for $A_{(1,2)sh}$ will take:

$$A_{(1,2)sh} = \frac{1}{\frac{1}{A_{1,2}} + \sum_{i=1}^n \frac{F_1}{F_{shi}} \left(\frac{1}{A_{shi(inner)}} + \frac{1}{A_{shi(outer)}} - 1 \right)};$$

where $A_{shi(inner)}$ and $A_{shi(outer)}$ - the absorption coefficients of inner and outer surfaces of the i -th shield, respectively.

Using these formulas, it is possible to determine the IR shielding configuration, that provides the minimum temperature of Body 1 (T_1), i.e. a sample with a quantum circuit.

The results of the calculations is verified using finite element simulations. Computer calculations is performed using COMSOL Multiphysics Heat Transfer in Solids and Surface to Surface Radiation. A two-dimensional axisymmetric model (see Fig. 6) was constructed to simplify calculations. We use the same surface absorption coefficients in the model for all the calculated scheme ($A_{Si} = 0.77$, $A_{Al} = 0.057$, $A_{Cu} = 0.0134$, $A_{Au} = 0.0479$, $A_{Absorp.coat.} = 0.9524$). The declared heat dissipation power is $3.45 \cdot 10^{-9} \text{ W}$. The temperature of the lower plate of the cryostat is fixed at 0.01 K . Two cases were considered, when the heating source is a superconducting quantum circuit itself (SQC, Fig. 5), and an external heat source (HS, Fig. 5). All the temperatures are normalized relative to the highest temperature, which we have got in all the simulations. The shown simulation result is the final temperature of a superconducting quantum circuit after stabilization for different shielding systems. The shielding system efficiency can also be estimated based on the minimum attainable temperature of

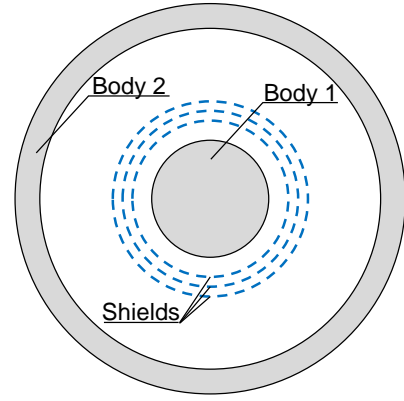


FIG. 4. Calculation scheme used for the heat transfer (by radiation) calculations between two bodies with an arbitrary number of shielding elements.

the sample.

In Fig. 5 we introduce the following designations: "SQC" – superconducting quantum circuit, "SH" – sample holder, "FS" – first shield, "SS" – second shield, "HS" – heat source in the form of an IR filter, and "C" – can on the lower stage of the fridge.

We considered seven shielding configurations with the increased complexity (weight and cost). Shielding configuration "A" consists solely of the sample holder and the can on the lower stage. This represents the simplest possible configuration. Shielding system "B" incorporates an absorbing coating on the can the can. Comparison with system "A" enables evaluation of thermal radiation absorption effectiveness of the lower cryostat stage shield. Configurations "C"-"E" examine different absorbing coating placements: "C" – outer surface of sample holder; "D" – outer surface of sample holder; "E" – both surfaces. These configurations, compared with "A", determine optimal coating placement on the sample holder. Configuration "F" adds a shielded enclosure with inner absorbing coating around the optimal sample holder configuration (selected from "A", "C"-"E"). This tests the effectiveness of the shield with absorbing coating surrounding the holder. Configuration "G" introduces a second shielded layer with absorbing coating. Comparison with F assesses the benefit of additional shielding layers.

The theoretical calculation and modeling results for the shielding systems with various absorbing coating positions are represented in Fig. 6 and demonstrate similar results with a mean difference of approximately 6.1%. The sample temperature is represented in relative units in order to demonstrate its temperature dependence on different shielding configurations relative to the worst-case shielding.

Based on the results, it can be seen that the nearest surface to the sample has a significant influence on its temperature. In our case, it is the sample holder lid, that is why it should have an absorbing surface. Starting from the "E" shielding configuration, it can be seen that the sample temperature is not changing (for shielding configurations "E", "F", and "G"),

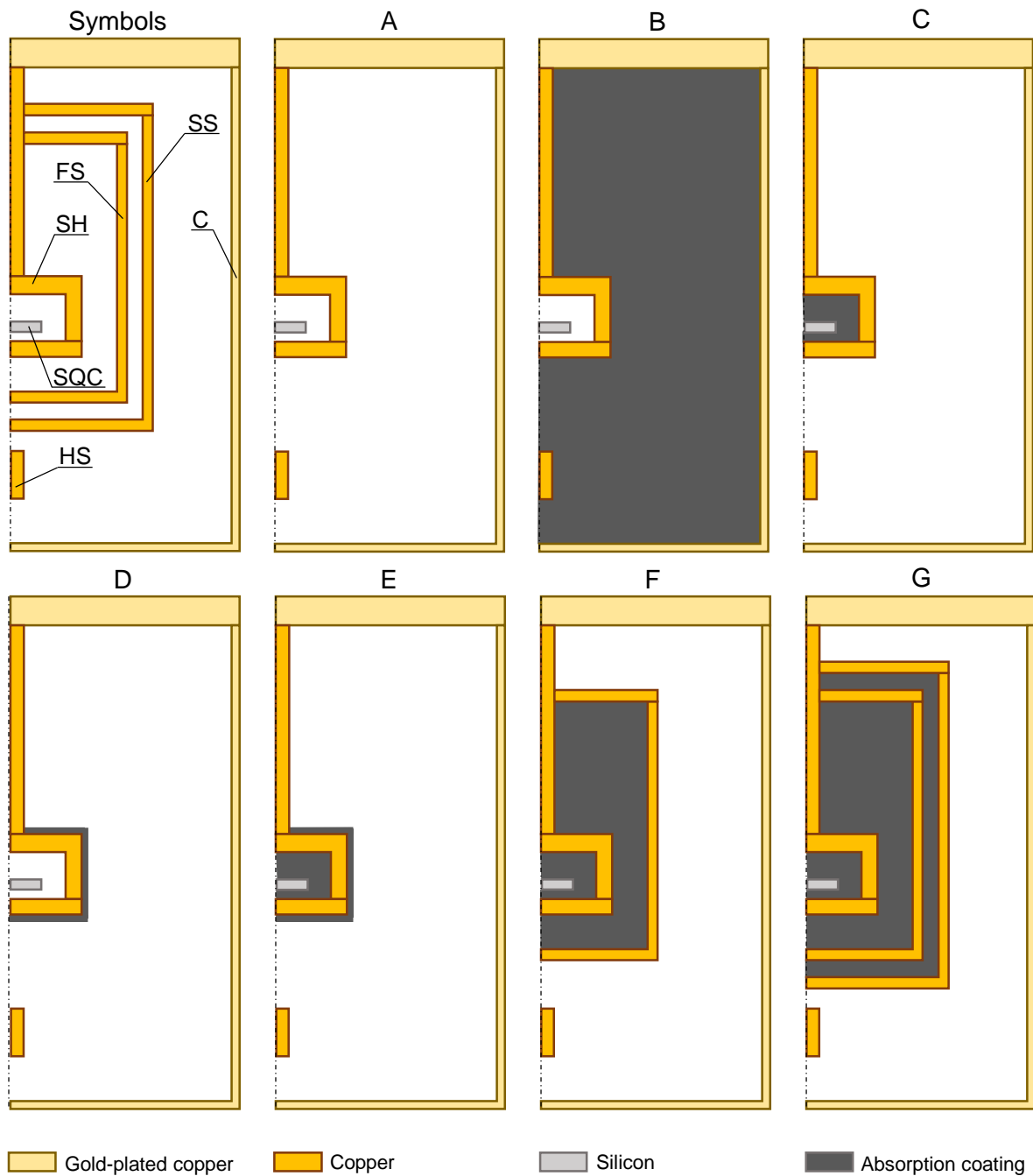


FIG. 5. Shielding system simulations: symbols and simulated configurations. Shielding configurations: A – copper sample holder with gold-plated copper can around the lowest temperature stage of a fridge (no absorption coatings); B – copper sample holder with the can with absorption coating; C – copper sample holder with an inner absorption coating with the can (no absorption coatings); D – copper sample holder with an outer absorption coating with the can (no absorption coatings); E – copper sample holder with both side absorption coatings and the can; F – sample holder (inner absorption coating) with additional shield around the sample holder (inner absorption coating) and gold-plated copper can; G – sample holder (inner absorption coating) with two additional shields around the sample holder (inner absorption coating) and gold-plated copper can. Symbols: SQC – superconducting quantum circuit; SH – sample holder; FS – first shield; SS – second shield; C – lower stage can of a fridge; HS – heat source.

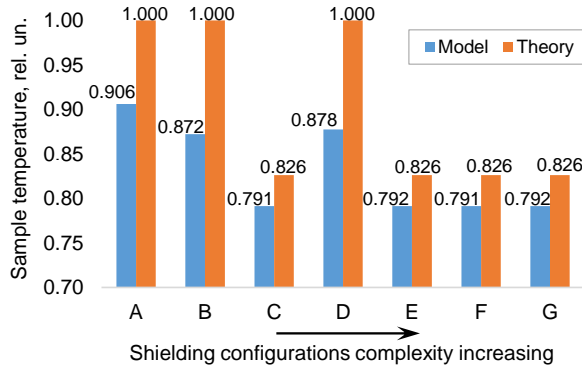


FIG. 6. Calculated sample temperature for different shielding configurations (simulations and theoretical results).

i.e., a further increasing of IR shielding quantity does not lead to an improvement in the shielding effectiveness. Therefore, an additional IR shields in the shielding system are unnecessary, as the IR protection provided by the sample holder lid appears to be sufficient. Another important conclusion that follows from the above discussion is that the sample holder itself is also a shielding system component, and should therefore be considered along with the shields.

According to our review, for a high effectiveness IR shields must be light-tight⁸⁰. At least in a half of considered papers, where the shield's shape is indicated, they consist of a cup with a lid^{18,70}. In some studies, there are special mentions, where the IR shield is hermetically sealed⁸¹, light-tight^{72,82,83} or the connection between the shield and the lid is sealed by the indium wire^{81,84}. Much less frequently, cylinder-shaped inserts are used^{51,81}, in rare cases, an individual shield may be used above the SQC⁵ or around it in the form of a tube^{49,69,85}. Technically, in order to ensure a light-tightness (or "IR-radiation-tight"), IR shields can be effectively integrated into standard dilution refrigerators, when they are designed as a cylinder with a lid. The connection between the cylinder shields and the lid can be threaded and easily sealed using the indium wire, and control wiring can be dropped into the shielded space through hermetic connectors in the lid. From the one hand, it is important to avoid any gaps (comparable to IR wavelength) between the lid and shields to ensure IR-radiation-tight solution. From the other hand, one should think on special form designed path for pumping down the shielded space.

e. Sample holder as an essential component of IR shielding. We have previously demonstrated that sample holders play an important role in IR shielding. Therefore, let's consider various types of sample holders that are described in the literature.

In order to ensure a robust thermal contact, approximately in a half of considered papers, oxygen-free copper^{24,86–89} is used (see Fig. 7). The choice of a copper is justified by its high thermal conductivity. The holders manufactured of superconductors, such as aluminum^{68,82,90–92}, considered in the other half of considered papers. The use of superconductors

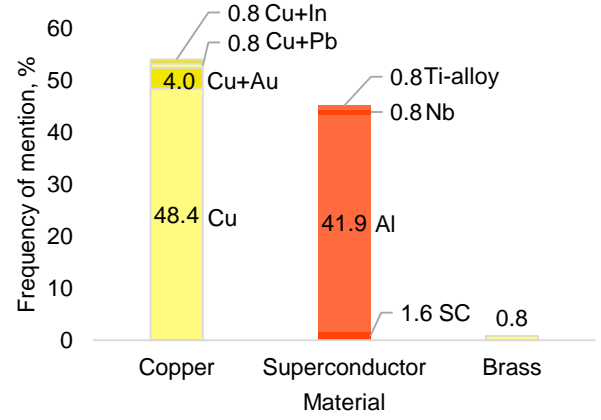


FIG. 7. Typical materials used for sample holders.

creates additional magnetic shielding owing to the Meissner effect (more detail consideration of this effect will be done later). Apart from aluminum, niobium⁹³ or titanium alloy⁹⁴ can also be used as superconductors, although such instances are rare. Despite the added protection from the magnetic field, superconducting sample holders have a lower thermal conductivity compared to the copper sample holders, that is why the use of the superconductors is undesirable. There are also copper sample holders coated by superconductor (lead⁹⁵ or indium⁷⁹). These sample holders create additional magnetic shielding while maintaining the high thermal conductivity. However, these examples are not common. There are also a few cases, where a copper coated with gold is used^{96–98}. The gold coating prevents the formation of the oxides on the copper, thereby reducing dielectric losses⁹⁹.

Among the works, where the shape of the sample holder is shown, approximately in a half of them the transmon qubits housed in a three-dimensional cavity^{100–104}, which serves as both a chip holder and a qubit circuit element for readout. The remaining works have three types of sample holder shapes: approximately 20% use the rectangular holders^{105–107}, 16% use the cylindrical holders^{108–110}, and 11% use a flat copper bases with printed circuit boards (PCBs) and lids above the chip^{18,61,99}.

The selection of a sample holder's shape depends on the SQC design and the wiring method to the cryogenic setup. Only the quality of the sample holder internal surface and its sealing are of importance.

In considered articles, just 6% of the sample holders have the lid with an IR absorbent coating. This solution is in good agreement with our calculations performed earlier. For this purpose, Stycast epoxy with additional SiC particles¹⁰⁵, a mixture of SiC and finely dispersed carbon powder⁴⁴, or Eccosorb CR-124 electromagnetic absorber^{23,71} can be used. The absorbing coating on the inner surface of the sample holder allows for more efficient cooling of the SQC, and at the same time it is also important that the holder has a high thermal conductivity. However, high dielectric loss of the absorber can affect qubit's coherence if they are close to each other. IR absorber should be positioned sufficiently far from

the qubit. Sufficient distance can be determined using surface participation method^{97,111}. This approach shows that the minimal qubit-absorber distance should exceed 4 mm. The surface participation method allows to quantify the extent to which the absorber interacts with the qubit's field in terms of maximal possible coherence time T_1 that can be achieved in presence of the dielectric loss channel:

$$\frac{1}{T_1} = \frac{\omega}{Q} = \omega p_{abs} \tan \delta_{abs} + \Gamma_0; \quad (2)$$

where T_1 , ω , and Q are coherence time, angular frequency and quality factor, respectively. $\tan \delta_{abs}$ is the dielectric loss tangent of the absorber, p_{abs} is a participation ratio of the material (a fraction of electromagnetic field energy stored within this material). Γ_0 represents other loss channels. The simulation conducted with a typically sized floating transmon¹¹¹ and a usual transmon on a lossless substrate in a lossless chip cavity to ensure $\Gamma_0 = 0$. Inner side of the top lid was covered with RF absorber with thickness of 0.5 mm and $\tan \delta_{abs}$ of 0.05, which is an upper bound for STYCAST IR absorber. During the simulation distance between the qubit and the bottom surface of the absorber was varied from 0.5 to 5 mm. The modelling shows that the influence of the absorber becomes as low as an influence of dielectric losses in silicon (limiting T_1 more than 10 ms) substrate when STYCAST is more than 4 mm away from the qubit (see Fig. 8). This ensures that the benefits of efficient cooling provided by the absorber are not compromised by degradation in qubit coherence.

In some cases, a weakly magnetic Eccosorb foam⁷⁶ may be used wrapped around the holder to absorb electromagnetic waves. However, without a base with a high thermal conductivity this foam may not be cooled sufficiently leading to re-emission of absorbed radiation into the SQC. In 3% of the works reviewed, a seal is used^{57,105,112} (particularly, indium wire¹¹³) to ensure light tightness.

The connection of the sample holder and the lid is critical. In order to determine the optimal method of connecting the sample holder to the lid, we have modelled and analyzed their different connection implementations. Three variants of the lid for the cylindrical sample holder have been considered and corresponding models have been developed (see Fig. 9a). The lid can either be common to the entire sample holder, including the chip, printed circuit board (PCB), and microwave connectors, or it can be individual covering only the sample with SQC. For the "standard lid", the connector as a heat source (Heat source 1) is located inside the sample holder, and there is also an external heat source (Heat source 2), which can be the element of the measurement circuit, e.g. microwave filter. This model corresponds to the lid that covers the chip along with the PCB and connectors. For "individual lid", both heat sources are located outside the sample holder.

The "individual lid with overlap" has an additional overlap to prevent radiation from penetrating through the gap (see Fig. 9a). The gap between the lid and the sample is varied from 0 to 1 mm in increments of 0.1 mm. As well as for an IR shielding modeling, relative units were used to represent the sample temperature.

Modeling results (Fig. 9b) demonstrate, that for a standard lid the sample temperature is approximately twice as high as compared to individual lid. The sample temperature increases gradually depending on the gap size. When choosing an individual lid, it is necessary to provide that there is no gap between the lid and the sample holder, because even 0.1 mm gap elevates the sample temperature by 12% in the case of individual lid with overlap (or by 37% in the case of usual individual lid). These simulation results demonstrate the necessity of using an indium wire seal between the sample holder and the lid, that allows filling all small gaps and surface irregularities and so eliminate it. An individual lid with an overlap provides a lower sample temperature, especially about 26% lower than that at a standard individual lid.

To summarize, the sample holder for the SQC should be made of a copper (or a copper coated with aluminum), and the inner surface of the holder should be coated by Stycast epoxy mixed with 1 mm SiC particles. Additionally, the sample holder lid of should be sealed with an indium wire to ensure light tightness.

B. Protection from electrical and magnetic fields

1. Shielding principle

Generally, protection from electrical and magnetic fields consists of three components: electrostatic shielding, magnetostatic shielding, and electromagnetic shielding (Fig. 10). The principle of shielding from an electrical field (Fig. 10a) involves the accumulation of the charge from a free space on the shield and its subsequent leakage into the ground. For effective protection against an electrical field, the shield must be made of a highly conductive material, such as copper or aluminum, with high-quality electrical grounding to minimize the contact resistance with the ground.

The shields made of ferromagnetic materials, such as permalloys (μ -metal, a soft magnetic alloy, or steels), with a high relative magnetic permeability (μ_r) are used to protect from a static and slowly varying (up to 1 kHz) magnetic field. In these shields, the lines of magnetic flux pass along the walls (see Fig. 10b), which have a lower magnetic resistance than the surrounding air. The shielding effectiveness is determined by magnetic permeability of the material the shield is made of.

The operation principle of the shields protecting from an alternating high-frequency magnetic field is based on an alternating electromagnetic field excitation within the shield. It creates alternating induction eddy currents (also known as Foucault currents). These currents shield the volume which this currents surround: the field inside the shield is brought down, while the field outside the shield is enhanced (see Fig. 10c). As a result, the field strength is reduced inside the shield and increased outside, thus leading to the field to be pushed from the shield. This type of shielding depends on the depth of field penetration at various frequencies (known as the "skin

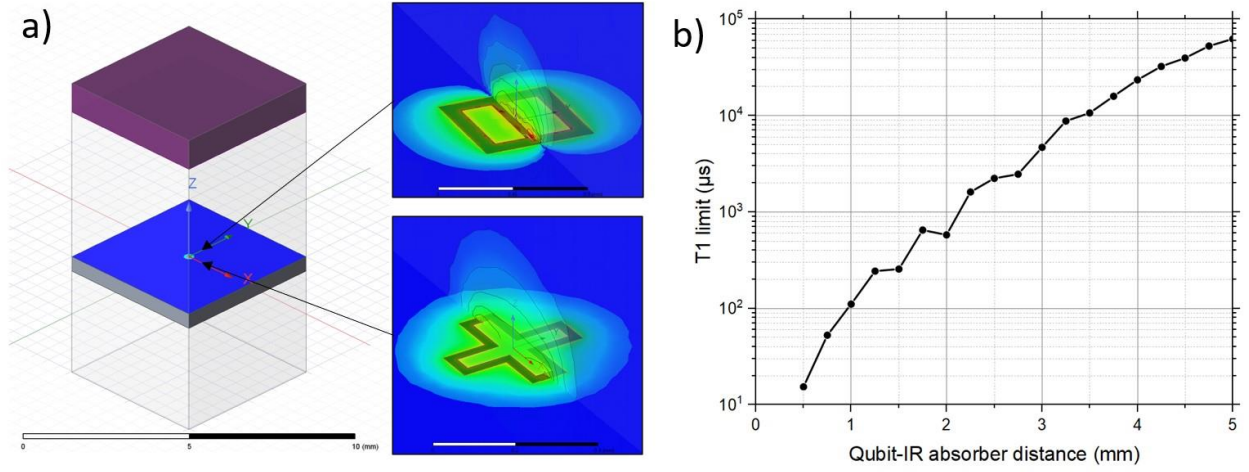


FIG. 8. a) Electric field distribution in superconducting qubit cavity for transmons of various types. Length of the size mark on transmon pictures are 0.8 mm for floating qubit (upper inset) and 0.4 mm for transmon qubit (lower inset). IR absorber is depicted as violet area; b) Maximal possible T_1 time vs qubit-IR absorber distance.

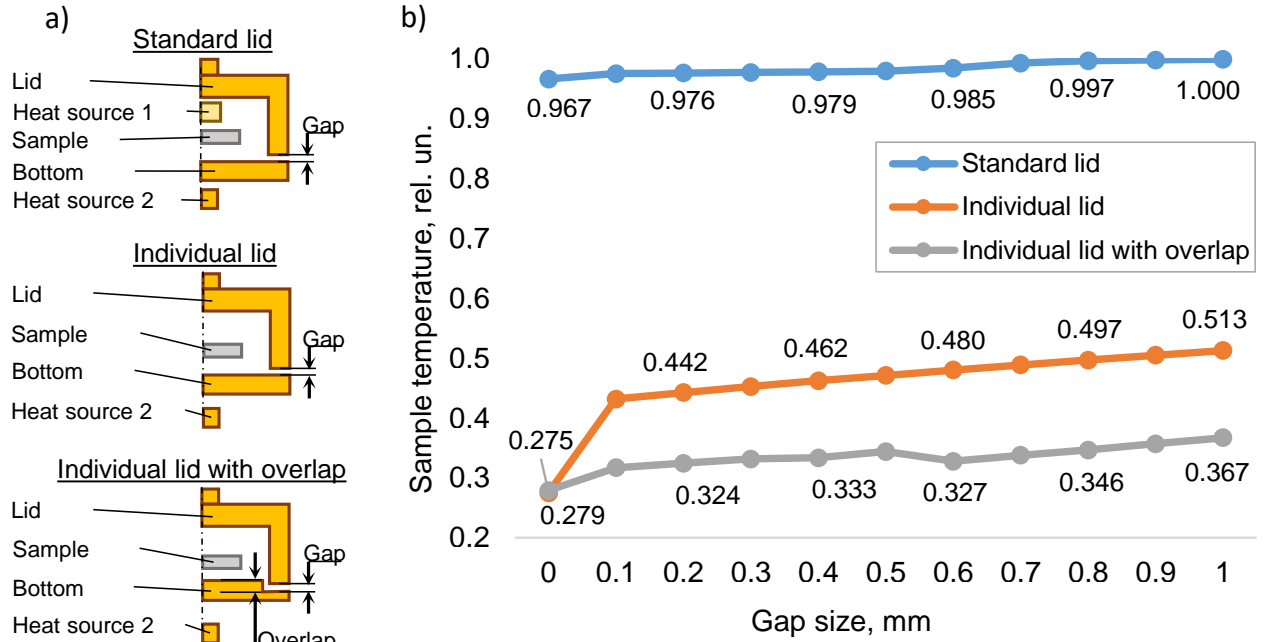


FIG. 9. Sample temperature versus gap size for different lid implementations: a) different holder designs; b) simulation results.

depth"), and becomes effective above frequencies (f) 1 kHz . The lower the skin depth (δ) the thinner (the lighter) the shield can be made:

$$\delta = \sqrt{\frac{\rho}{\pi f \mu}}. \quad (3)$$

Non-magnetic materials with low resistivity (ρ) or ferromagnetic properties with high permeability (μ), such as copper, aluminum, μ -metal, and steel are used to design the shields, which resist the penetration of the EM field. For example,

skin depth of the copper at 100 kHz equals $200 \mu m$.

Superconductors also provide excellent protection against alternating electromagnetic fields, as in an ideal conductor the currents flow on the surface without penetrating deeply into the metal, i.e. low skin depth. Ideally, such shields should have no holes or slots.

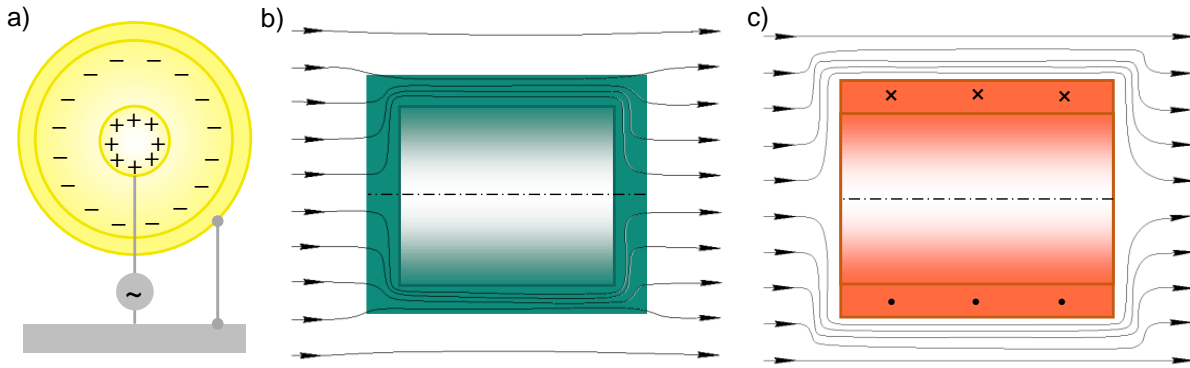


FIG. 10. The shields operating on different physical principles: a) electrostatic – the external shield is discharged due to the connection to the ground; b) magnetostatic – magnetic field is concentrated in the ferromagnetic loop; c) electromagnetic – external alternating electromagnetic field, induces eddy currents in the shield loop which compensate electromagnetic field inside the shield.

2. Requirements for shielding from electromagnetic fields

Based on the discussed above theory of protection from electromagnetic fields, the following requirements can be summarized:

1. The shielding should protect from both electric and magnetic fields including constant and alternating high-frequency fields.
2. For electrostatic shielding, it is recommended to use the materials with a high electrical conductivity and robust grounding properties. Recommended materials are copper and aluminum, as they have high thermal conductivity, provide RF shielding and are widely available.
3. For magnetic shielding, it is recommended to use a metal with a high relative magnetic permeability (greater than or equal 100,000).
4. For electromagnetic shielding, it is recommended to use a superconductor (such as aluminum) or a non-magnetic metal with a low skin depth (for example, copper or aluminum).

3. Practical implementation of electromagnetic shielding

Now, we will discuss various implementations of electromagnetic shielding that are currently known.

a. Superconducting shields. Superconducting shields used for protection from parasitic magnetic fields are primarily manufactured from aluminum (Fig. 11)^{68,100,114–117}. Other superconducting materials that were found in the literature: lead^{42,95,118}, tin¹¹⁹ or their alloys^{105,120}, niobium¹²¹ and indium³⁹. Aluminum is preferred material for superconducting shielding due to the ease of its workability and relatively low cost compared to other materials.

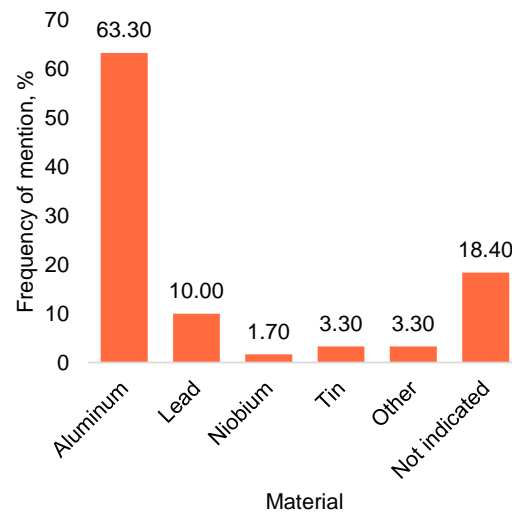


FIG. 11. Typical materials used for superconducting shields.

In considered papers, almost a quarter of all superconducting shields in combination with an IR shielding, which are coated with an IR-absorbing material, are used (Fig. 12a)^{5,70,119}. These shields usually consist of a light tight cup with a lid^{18,70}, which allows for more compact shielding due to the possibility of combining together IR and magnetic shielding (shielding from magnetic field). However, superconductors have a lower thermal conductivity than in its normal state. It has a negative impact on the absorbed heat dissipation, which is crucial for IR shielding. To effectively cool a superconducting shield, a superconducting layer can be placed on a copper base (Fig. 12b)^{39,119,120}.

Cup-shaped shields without a lid^{37,122} or individual shields placed over the chip⁵ have also been presented. However, for a more uniform distribution of the magnetic field inside the

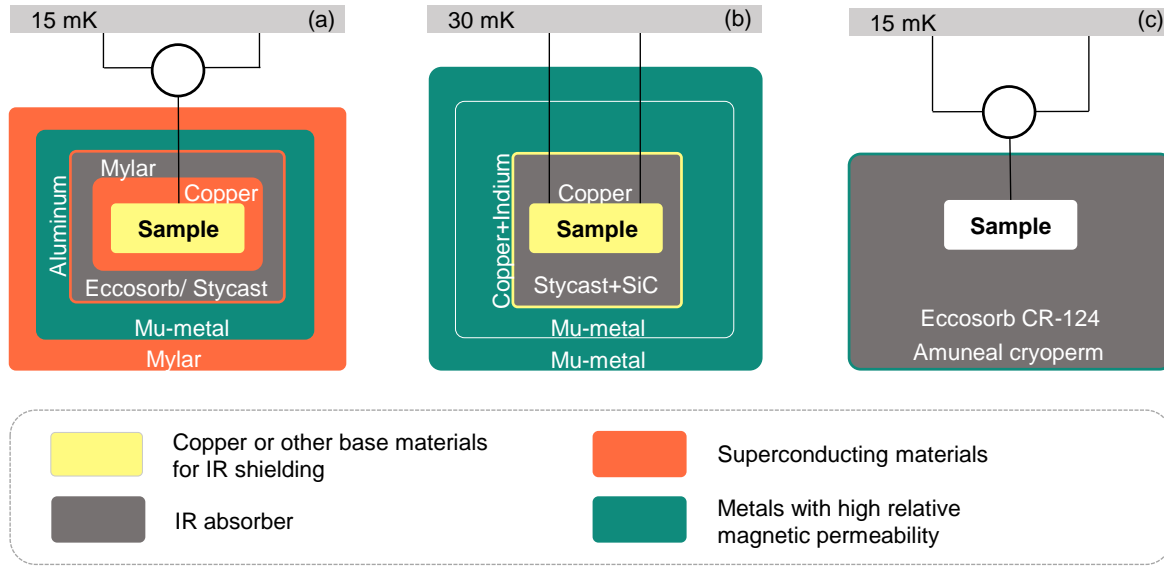


FIG. 12. Shielding systems with various IR shields: a) a 4-layer shielding with two IR-reflective Mylar layers and a combination of superconducting and IR shields¹⁸; b) a 3-layer shielding: a superconducting shield combined with an IR shield and double-layered μ -metal³⁹; c) a single-layered cryoperm magnetic shield in combination with an IR absorber⁴³.

shield, it is necessary to use tightly closed shields.

Based on the above analysis, we can conclude that a superconducting shield is an essential part for the shielding system. This shield can be realized by two methods:

1. A light-tight, one-layered aluminum superconducting shield surrounding the sample holder. This shield must follow after an IR shield.
2. A combined shield protecting from IR radiation and electromagnetic field, consisting of a superconducting layer on a copper light-tight shield coated by an absorbing material and surrounding the sample holder.

b. Material for magnetic shields. The operation principle of magnetic shielding is based on the magnetic field retraction into a shield material that has a high relative magnetic permeability (typically 100,000 or more)⁹⁹. These materials are typically made of ferrum-nickel alloys that have been subjected to special processing, such as annealing in a hydrogen atmosphere. In the literature, these materials are often referred to as μ -metals^{42,56,106,123,124} or they may have specific names (Fig. 13), such as Cryoperm^{112,125,126}, Cryophy^{50,114,127}, Amumetal^{69,79,117,128,129} (or Amuneal^{43,49,81}).

The presented materials differ in the method of their thermal processing in a hydrogen environment, and consequently, in their relative magnetic permeability (Table 2).

For these shields, it is preferable to use a material with the highest relative magnetic permeability. As an exception, an iron shield¹³⁰ can be used. However, its relative magnetic permeability is much less compared to μ -metals.

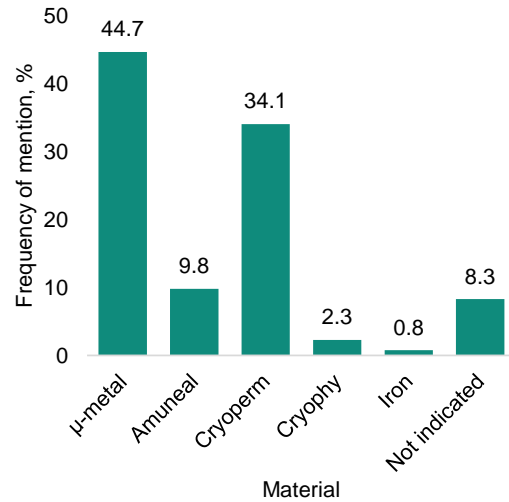


FIG. 13. Typical materials used for magnetic shields.

For magnetic shielding, cup-shaped shields are frequently used^{75,122}. Cylindrical shields with a lid^{89,131,132} are less frequently employed. Individual magnetic shielding is used in special cases⁵. As with superconducting shielding, the presence of a lid on the shield enables the equalization of the magnetic field within the protected space, thus it is recommended to use the magnetic shield with a lid.

Magnetic shields can also be combined with IR shielding (Fig. 12c)^{43,59,72}, but it was found only in 6% of consid-

TABLE II. The relative magnetic permeability of various magnetic materials.

Material	Relative magnetic permeability, μ_r
μ -metal	80,000-400,000 ⁴⁸
Cryoperm 10	65,000-250,000 ¹³³
Amumetal	60,000-400,000 ¹³³
Cryophy	₁₃₄
Iron (99.8% pure)	5,000 ¹³⁵

ered papers. Such combination of shielding methods is not justified due to the low thermal conductivity of a μ -metal compared to a copper, and can lead to a poor cooling of the absorbing coating. In some studies, specific guidelines are provided for the use of magnetic shields. For example, it is recommended not to include magnetic components inside the shield^{131,136,137}, or the sample holder should be placed closer to the bottom of the shield⁸⁹, and a thermal anchor should be installed on the shield to improve its cooling^{70,132}. Some magnetic shields have special design features such as waveguides on the lid^{61,127} or light tightness^{56,72}. These design features help to minimize the influence of the magnetic field on the SQC. Almost a half of considered shielding systems have the sample holders with special features. Either the holder itself is made of a superconductor^{109,138,139}, or it has superconducting^{18,95} or absorbing layers^{23,71,105}. These aspects have been discussed in more details before in a section about sample holders.

c. The number of layers, the shape and arrangement of the electromagnetic shields. Based on the recommendations presented above, it is possible to choose materials for electromagnetic shielding. However, it is also very important to determine the configuration of shielding, i.e. the arrangement and number of shield layers. In order to determine the optimal order of magnetic and superconducting shields for maximum shielding effectiveness, we simulated the magnetic field distribution within cylindrical shields.

The magnetic field was simulated using the finite element method. Two cylindrical shields were considered, nested one inside the other. The shields were placed in a vacuum parallelepiped. The external magnetic field of 50 μT along the axis of the cylinders was set. Relative magnetic permeabilities were assigned for the μ -metal (70,000), superconductor ($1 \cdot 10^{-6}$), and vacuum (1). Magnetic induction distribution in the area was simulated. The thickness of the shields is set to 1 mm. Outer diameters of the shields are 66 mm and 70 mm. The heights are 180 mm and 190 mm. The calculation scheme and simulation results are presented in Figure 14. In the double-shield configuration, the minimum wall-to-wall separation between shields was maintained at 2 mm.

Based on the modeling, the combination of aluminum shield inside and μ -metal shield outside can provide a minimum level of magnetic field at the SQC position inside the shields. The combination of magnetic shields should be chosen based on the required level of the external magnetic field.

We recommend positioning the shield assembly as close as possible to the sample holder while maintaining minimal

shield distances. It reduces the residual magnetic field in the sample space and enables more efficient use of the limited available space in the cryogenic environment.

C. Additional protection against high-energy radiation

In certain studies, there have been identified specific shielding techniques for reducing the impact of high-energy radiation, such as cosmic rays. This type of radiation has a high penetrating power, making it difficult to protect SQC from it. In^{140,141}, lead bricks were placed around the dilution refrigerator at room temperature as a part of the shielding system. These bricks do not act as superconducting shields, but rather as a barrier against X-rays and cosmic radiation. Alternatively, in some cases the dilution refrigerator could be located deep underground¹⁴¹, or in a room carefully shielded against electromagnetic radiation^{116,142}. Although these methods help to additionally reduce the amount of radiation incident on the SQC, they require more sophisticated implementation.

D. Shielding configurations known at present

Let's consider and analyze the existing shielding systems according to the previously discussed recommendations. Various configurations of multilayered shielding systems are illustrated in Fig. 15. Two cases are presented in histogram: in the first case the sample holder is considered as a part of the shielding, and in the second it is not. The shielding configurations in Fig. 15 represent the order of shields used: starting from the sample holder (or the first shield) and finishing with the last shield within the system.

We would like to emphasize that the frequency of shielding systems mention in literature does not necessarily correlate with optimal performance. The subsequent analysis in this section aims to justify the prevalence of specific shielding configurations in the literature based on the presented in this paper simulation results.

Shielding from IR is predominantly accomplished with a single layer. Two layers of absorbent coatings are used in only 10% of cases^{73,74,122}, provided that we do not take into account the sample holder. The rationality of using just one shielding layer is also supported by our modeling results (see Fig. 6). However, taking into account absorbent coatings on the sample holder, we can find that most shielding systems employ two IR layers (Fig. 15). According to our calculations, the sample holder inner surface plays a significant role in protecting SQC from IR radiation. To simplify the shielding system design, an absorbing coating can be applied only on the inner surface of the sample holder, without using an additional IR shield around.

Approximately in 80% of considered works IR shielding is located around the sample holder (Fig. 16a)^{38,51,55,68,85}. In other cases it surround the coldest plate of the fridge as

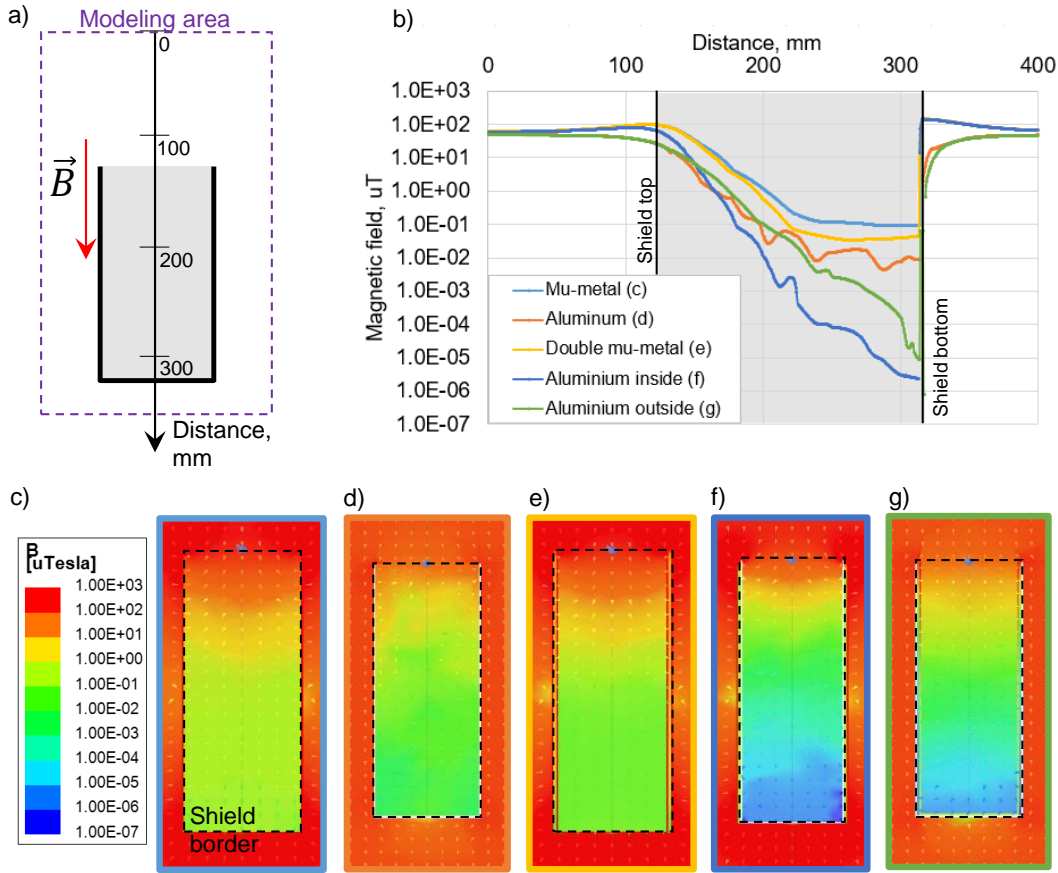


FIG. 14. Simulation of magnetic field distribution within cylindrical shields: a) calculation model (the external magnetic field of $50 \mu T$ directed along the axis of the cylinders); b) comparison of magnetic field strength along the shield axis for various shielding configurations; magnetic field distribution within: c) single μ -metal shield (color bar screenshot from COMSOL for magnetic field strength is also valid for d)-g) configurations; the boundaries of the simulated shields are indicated by a black dashed line here and on the d)-g) various configurations: d) single aluminum shield, e) double μ -metal shield, f) aluminum shield surrounded with a μ -metal shield, g) μ -metal shield surrounded with an aluminum shield.

shown in Fig. 16b^{37,122}. IR shields are typically positioned immediately after the sample holder^{58,85,126,127}. However, in multilayered shielding systems, they can be located at second (Fig. 16c)³⁷ or even fourth^{66,122} shielding layer. Modeling results show that the multilayer IR shielding have the same effect as a single-layer one.

Only 12% of superconducting shields have two layers^{122,143,144}. This is well explained by the simulation results, according to which the number of superconducting shielding layers does not affect the shielding quality. The authors in¹⁴⁵ state that the use of a superconducting shield with a μ -metal shield can achieve a magnetic field level of approximately $1 nT$. It is also supported by the modeling results presented above. The provided magnetic field is sufficient to protect the SQC from external magnetic field fluctuations. From Fig. 15, it can be seen that the majority of superconducting shielding is realized by the sample holder, what is another way for simplify the shielding system.

The location of the superconducting shields may vary, most of them directly surround the holder^{68,121,128}, while the

others located either at lower^{37,122} or penultimate stage of the fridge¹¹⁹. Due to the requirement of the magnetic field to be uniformly distributed at the sample holder place, it is preferable to close the superconducting shield by the lid.

Superconducting shields may be located either right after the holder (Fig. 17a)^{40,117,144} or after IR shield^{85,121,127}.

In systems with more than four shields, a superconducting shield may be placed at third layer from the holder⁷³, or even at fifth^{37,122}. However, our modeling results showed that multilayered shielding system do not significantly increase shielding efficiency, so a more compact design may be used.

In approximately in 80% of considered works, single-layer magnetic shielding was used, in 19% two-layer shielding was used^{42,106,114,146}, and only in one work⁸⁶ presented three-layer shielding was used. As it was previously demonstrated, the combination of a superconducting shield inside and a μ -metal shield outside provides the most effective protection against magnetic fields.

As well as the other types of the shields, magnetic shields are typically placed around the holder^{37,75,147-149}. At the same

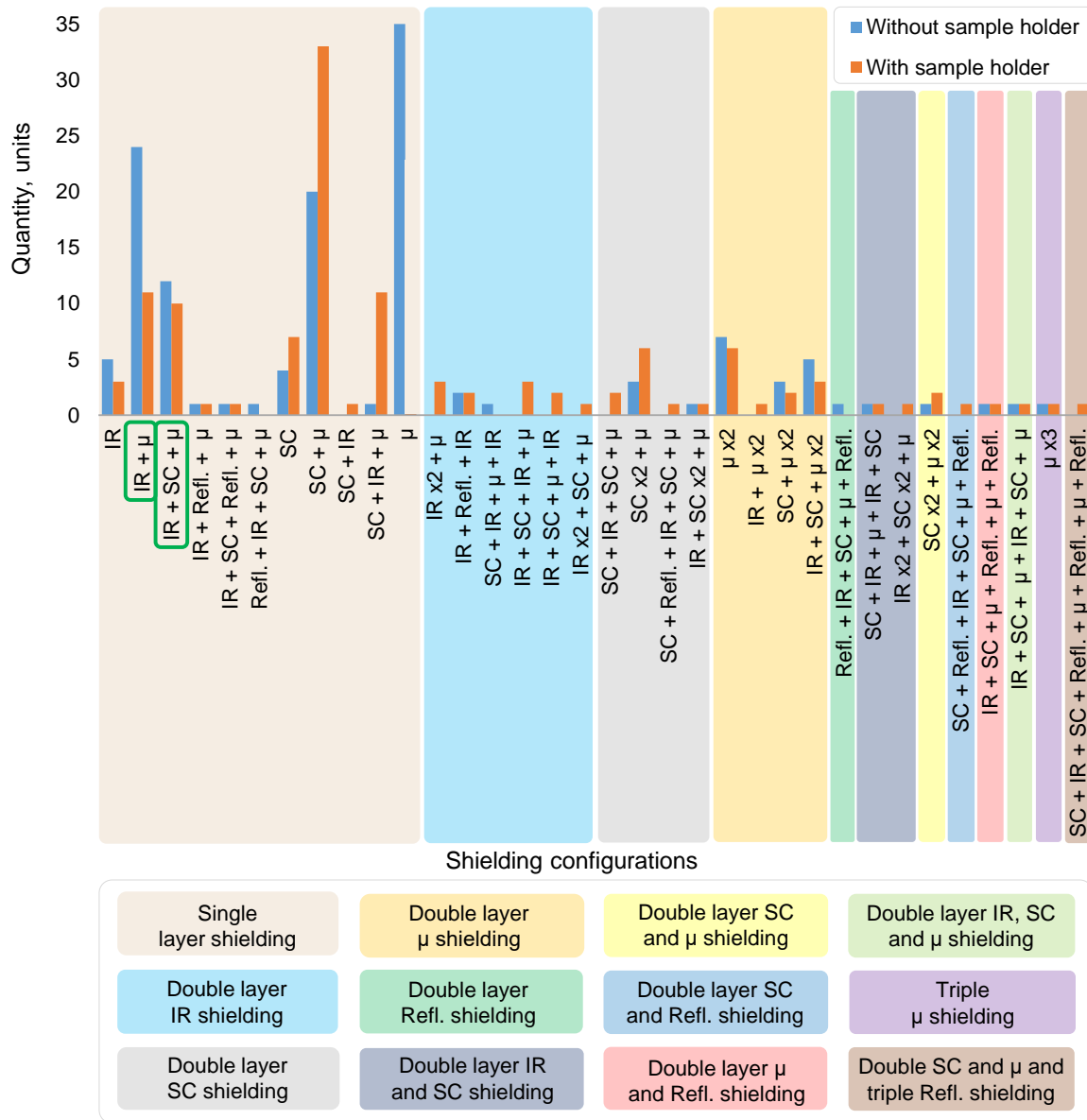


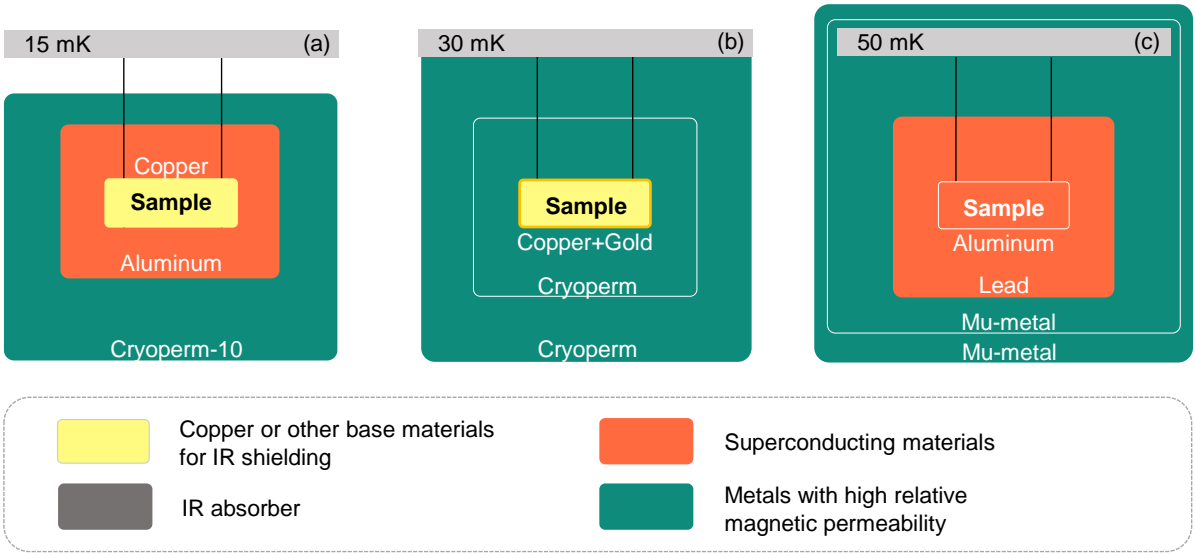
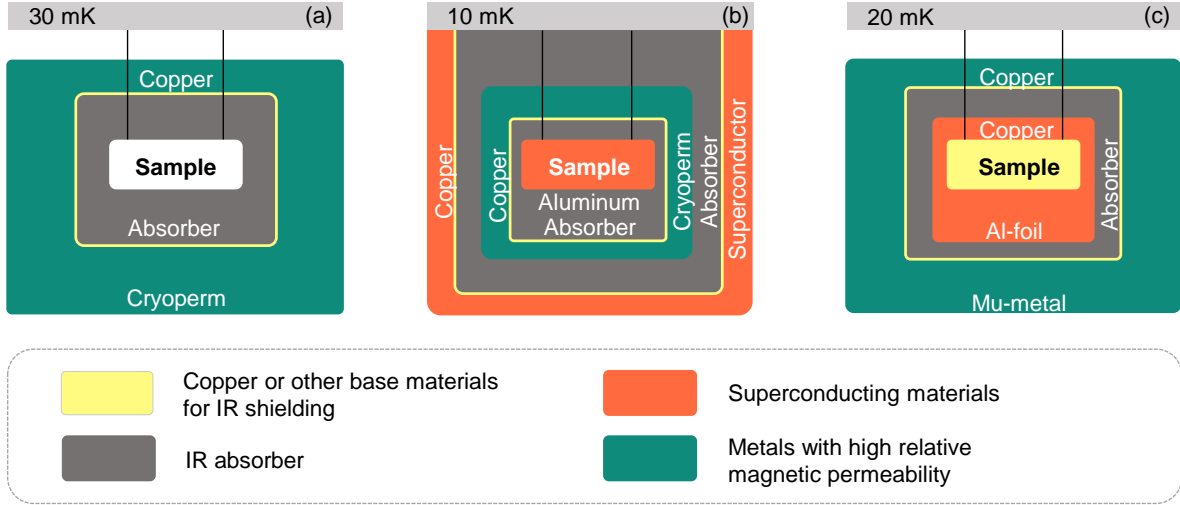
FIG. 15. A review of shielding configurations. “SC” – superconducting layer, “IR” – infrared radiation absorbing layer, “μ” – high magnetic permeability layer, and “Refl.” – reflective infrared radiation layer. “Quantity” is the number of referenced papers employing each specific shielding configuration.

time, there are more options for the location of magnetic shields within the fridge, such as the lower stage (Fig. 17b)^{68,123}, 2.7 K¹¹⁹ or 4 K^{44,142}, or around the fridge itself (Fig. 17c)^{23,100,144}.

How it was been determined in the modeling, there is requirement for the shield to be closed, so it may only be placed around the sample holder. In case the magnetic shield is the only one shield used in a system, it typically follows right after the sample holder^{150–152}. In other cases, the magnetic shield may be placed outside of the other shields, such

as IR shields^{49,60,126} and superconducting shields^{52,114,144}. However, in case of multilayered magnetic shielding system, μ-metal shields may be inserted between the superconducting shields^{37,122}. As it was previously mentioned, for optimal shielding performance, the superconducting shield should be placed inside the μ-metal one.

Most considered shielding systems meet our requirements for the shielding. Requirements description for the shields based on the modeling results make it possible to identify excessiveness in the shielding system and make it lighter



and more compact. We also mark on Fig. 15 (by a green frame) the best shielding systems based on our simulation results. If it is possible to use all three types of shields, we recommend to use “IR + SC + μ -metal” system. If, due to some limitations, it is possible to use only two shields, we recommend the system “IR+SC”, the less preferred configuration is “IR+ μ -metal”.

III. MICROWAVE LINES FILTERING

As previously mentioned, the optimal protection of SQCs from stray electromagnetic fields can be achieved by the use of shielding in combination with microwave filtering. In the following paragraphs we’ll investigate in more detail the different types of filtering and consider their applications in existing cryogenic setups.

All control lines of SQC (here we are focused on SQC based on transmon qubits) can be divided into four categories:

1. Readout input lines. The typical frequency band for these is from 4 to 8 *GHz*, power required for single qubit readout is around -110 *dBm* in the case of system without on-chip purcell filters. In multiqubit systems one readout line can be used for readout several (up to 10) qubits, so in this case the power coming on chip is around -100 *dBm*.
2. Readout output lines. The typical frequency band for these is from 4 to 8 *GHz*, typical power coming from chip to the first stage amplifier is around -115 *dBm* in the case of single qubit readout and around -105 *dBm* in the case of multiqubit readout. The main feature of readout output line is the necessary of minimizing signal losses from quantum chip to the first stage amplifier for improving readout efficiency, therefore it is undesirable to use attenuators or high-loss IR filter for it.
3. Drive lines (lines for performing arbitrary single qubit rotations). The typical frequency band for these is from 4 to 8 *GHz*, power required for fast single qubit rotations is around -80 *dBm*.
4. Flux lines (lines for in-situ tuning of superconducting qubit frequency). The typical frequency band for these is from DC to 500 *MHz* (in the case of fast flux-assisted two qubit gates), the values of DC current required to adjust the frequency is on the order of several *mA*.

For high performance of SQC it is necessary to filter the frequencies out of band for all the types of lines listed above. Insufficient filtering of frequencies close to the qubit ones can lead to parasitic single-qubit rotations, degrading the single qubit gate fidelities, as well as undesirable population of possible coupled with qubits parasitic modes, which can lead to additional qubits decoherence. Insufficient filtering of IR frequencies (above 90 *GHz*) can lead to cooper-pairs breaking in superconductor thin film and also degrade the qubit coherence. In this article we focus only on the different filter types used for all lines listed above. The purpose of other microwave components, used in control lines, such as attenuators, circulators, isolators etc., is described in detail in Ref.³².

A. Requirements for filters

Filtering is usually used to protect SQCs from stray electromagnetic fields and IR radiation that can propagate in microwave lines. For this purpose, various types of radio frequency (RF) and microwave (MW) filters (Low-pass filter - LPF^{5,39,85,100,153}, High-pass filter - HPF^{42,131,154} or Band-pass filter - BPF^{86,112,138}) covering the SQC operating range (typically, 4-8 *GHz*) are usually used. RF and MW filters are designed to cut off a portion of the signal spectrum outside the required passband, suppressing most of the stray electromagnetic fields. For suppressing IR radiation, a special IR filters are usually used. The working principle of such filters based on IR radiation power loss due to eddy currents excitation in filter filler material¹⁵⁵.

It is necessary to use RF and MW filters with IR ones, as they cut-off different parts of the signal spectrum. For this purpose, one can use BPF+IR or a combination of HPF+LPF+IR. However, in considered measurement circuits, it is more convenient to use either a single LPF or a single IR filter, or various combinations of these filters. The main requirement for IR filters is as low as possible attenuation in the SQC operating frequency range, smooth transmission characteristic and at the same time high enough attenuation (no less than 20 *dB*) at higher frequencies (above 20 *GHz*).

One of the important requirements for microwave components (attenuators, filters, etc.) when operating at millikelvin temperatures is the availability of efficient thermalization. The lack of proper thermalization can lead to a significant increase in the effective temperature of the qubits^{85,106}. The issue of thermalization, methods of increasing its efficiency and its influence on qubits effective temperature is considered in detail in^{106,156}, therefore, in this review we decided not to focus on this.

B. IR filters

In works, IR filters may have different designations (IR filter^{49,136,157,158}, lossy filter^{38,121,159}, thermalization filter¹¹⁹, etc.), but all of them are designed for the same purpose: to suppress stray IR radiation in signal lines. The filling material for such filters (see Fig. 18) typically consists of an epoxy resin containing fine particles of carbonyl iron (Eccosorb CR-110^{18,79,132,160}, or, less frequently, CR-124³²), and metal powder⁴⁴ (mainly copper^{83,142,161}). Other possible fillers include epoxy resin based on aluminum oxide (Stycast) mixed with bronze powder¹⁰⁵, or without it¹¹². Specific fillers such as carbon nanotubes may also be used¹⁰⁰.

There are no studies with a direct comparison of the IR filters efficiency with different types of filling material. However, in considered works, Eccosorb CR-110 epoxy is the most widely used in IR filters (see Fig. 18).

IR filters are employed in all types of signal lines of cryogenic setup. In the following paragraphs we will analyze various filtering configurations.

C. Filtering of input readout line

Typically, in cryogenic setups one^{43,60,86,101,130} or two filters^{55,128,157,158,162} are used at the input readout line. Less frequently, three filters are installed in a row^{109,161,163}. RF and MW and IR filters can be used both individually^{38,40,66,164} and together^{70,112,165}. Different combinations of filters for the input readout line are shown in Fig. 19.

In most measurement circuits, filters are located outside the shielding^{5,68,106,124,131,139}. Less frequently, they may be located both inside and outside the shielding^{37,39,137,138}. In very rare cases, the filters are only located inside the shielding¹¹⁹, mounted on the lid of the shield^{44,56}, or just prior to the sample holder¹⁴². In⁸⁵ it is indicated that the location of an IR filter inside the shielding can reduce the quasiparticles gener-

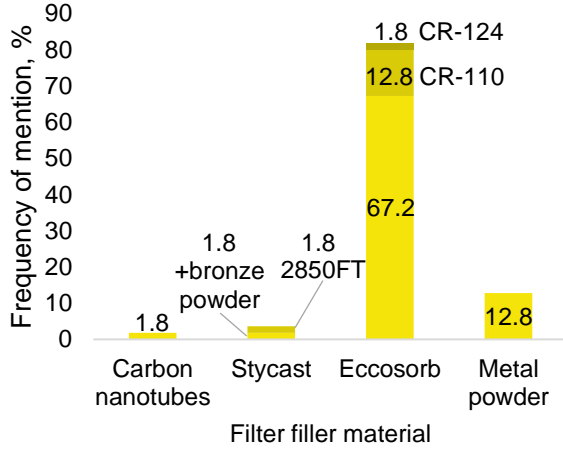


FIG. 18. Typical filling materials for IR filters.

ation in a qubit. Thus, it is recommended to place the IR filter within a metal shield thermalized on the base stage of the dilution refrigerator. For RF and MW filters there is no special requirements for placement in the measurement circuit. Thus, they are typically located outside the shielding.

As it was mentioned before, it is better to use RF and MW filters and IR ones together, the number of filters at the input readout line should be at least two. The recommended configurations should be the following: either BPF + IR or HPF + LPF + IR. For the filler of IR filters, Eccosorb CR-110 epoxy is the most popular material used in considered works.

D. Filtering of output readout line

The output readout line experiences the same types of radiation effects, as the input line. Therefore, for this line the same recommendations can be made as for the input readout line. For the output line, a little more variety of filter configurations are used. For instance, at the output readout line a combination of HPFs and BPFs are frequently used (see Fig. 19).

Typically, two filters are used, but there are also single filters or combinations of three different filters. As shown in Fig. 1, the filters are generally placed at the lower stage of the dilution refrigerator. In addition, we recommend to place only IR filters inside the shield thermalized on the coldest stage of the cryostat. The design and materials used for IR filters at the output line are the same as for the input one.

E. Drive line filtering (XY control)

For the SQCs driving, special drive lines are utilized. In some implementations, the SQC driving is carried out through a readout line. However, in this review, we will consider an individual drive lines separated from readout, and analyze their

filtration. At the SQCs drive line, the following filtering configurations are commonly used: LPF, IR, or LPF+IR (see Fig. 19). More complex combination (e.g. LPF+IRx2) is rarely used. BPF is also less frequently utilized on this line. These filters are often placed at the lower stage of the fridge, but they can also be placed at the 100 mK stage or at room temperature.

F. Flux line filtering (Z control)

The flux line filtering is usually based on application of LPF and IR filters. For this line, as for the drive line, we consider a separated flux line (in some implementations the magnetic flux can be manipulated by a special coil surrounding the sample holder). The most commonly used configurations of the filters on the flux line are LPF+IR, LPF or IR+LPF. Generally, the flux line filters are placed at the lower stage of the fridge, at the same time an LPF can be placed on other stages of the cryostat.

IV. METHODS FOR EVALUATING THE EFFECTIVENESS OF SHIELDING SYSTEMS AND LINES FILTERING

In order to select a shielding system, which can reliably protect from stray electromagnetic and IR radiation, an assessment of the shielding effectiveness should be done. The main challenge of selecting such system is that the system should be compact having a high shielding efficiency. The shielding effectiveness can be evaluated based on the measurements of specific parameters. The values of these parameters allow the quantitative evaluation of the incident radiation. Several techniques based on the SQC parameters measurement have been proposed in the literature. Based on our review, the following techniques are used: the resonators Q-factor evaluation, the SQC effective temperature measurement, the qubit energy relaxation rate measurement, and the estimation of quasiparticle tunneling rate. Let's briefly consider all of these methods.

A. Resonator Q-factor (Q_i)

A spontaneous IR radiation with energy exceeding the binding energy of a Cooper pair ($f \geq 2\Delta/h \approx 100$ GHz for aluminum thin films¹⁶⁶) can cause the breakup of a Cooper pair creating the quasiparticles. The resonator Q-factor depends on the density of quasiparticles in superconductor¹⁶⁷. Additionally, magnetic vortices may appear in an aluminum thin film under the influence of an external magnetic field, which can also reduce the Q-factor of resonators^{119,166}. Therefore, the Q-factor of a resonator can be an indicator of how much of spontaneous IR radiation and external magnetic fields reach the sample.

In¹¹⁹, different shielding systems were compared by the values of measured resonators Q-factor. The results showed that the addition of a cryoperm shield at the 2.7 K stage of the dilution refrigerator can increase the resonator internal Q-factor by a factor of two. However, to demonstrate this effect, the

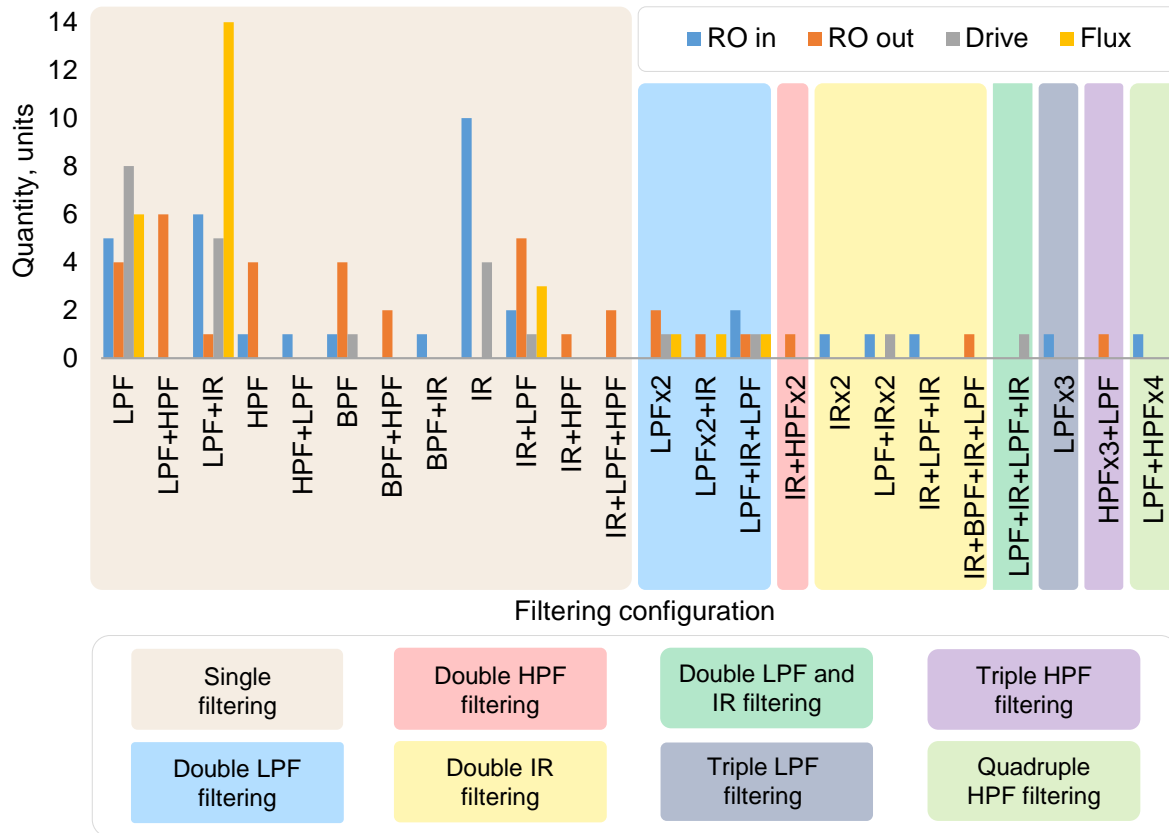


FIG. 19. A review of filtering configurations for readout (RO), drive, and flux lines. LPF stands for a low pass filter, HPF for a high pass filter, and BPF for a band pass filter. IR represents an infrared radiation filter. The “Quantity” represents the number of papers (from references list), which use the exact filtering type.

researchers created a magnetic field of about $200 \mu T$ inside the dilution refrigerator. The authors did not observe a significant improvement of the resonators internal Q-factor, while increasing the complexity of the shielding.

In⁴⁴, it was found that ensuring the light-tightness of the shielding system can be achieved by using an indium gasket between the shield and its lid, which lead to an increase in the Q-factor of a coplanar waveguide resonators from 10^5 to 10^6 . An important detail of this experiment was that the sample holder was surrounded by a shield with a relatively high temperature of 4 K. It is also should be noted, in some experiments in⁴⁴, a special heat source directly radiated the sample was used, which intentionally created a more challenging conditions for the resonators' performance.

Generally, the resonator Q-factor is not the best indicator for evaluating shielding effectiveness, because it requires an external magnetic field or IR radiation source, indicating that it has a low sensitivity.

B. Effective temperature of the quantum system (T_{eff})

In several studies^{33,168–170}, it has been noted that the measured excited state population (or effective temperature, T_{eff}) of a quantum system is significantly higher than the theoretical one. Such unexpected increase in the measured effective temperature is assumed to be due to the presence of nonequilibrium quasiparticles. The quasiparticles can be induced by a stray microwave noise, cosmic rays, or an IR radiation from warmer stages of a dilution refrigerator¹⁷¹. Therefore, the effective temperature of a qubit can be used as a metric for evaluating the effectiveness of the shielding from spontaneous IR radiation and stray electromagnetic fields. In Ref.¹⁷², the effectiveness of an IR shielding with two different absorbing coatings was evaluated based on the qubit effective temperature.

This method may be useful for determining the best IR absorber for the shielding, but it is probably not suitable for comparing different configurations of magnetic shielding.

C. Energy relaxation rate of the qubit (Γ_1)

It is known that the energy relaxation rate of a quantum system is composed of two components: the relaxation rate due to the quasiparticles, and the relaxation rate due to a combination of other factors such as radiation, cosmic rays, dielectric losses, and the two-level systems fluctuations¹⁴⁰. Having determined the contribution of each factor to the relaxation rate, it is possible to use this rate as a sensor for the normalized quasiparticle density. As mentioned earlier, the quantity of the quasiparticles is directly correlated with the amount of radiation. Using a calibrated radiation source, the contribution of other sources (cosmic rays, dielectric losses and two-level systems fluctuations) to the energy relaxation rate has been determined in¹⁴⁰. As a result of these measurements, it has been shown that protection from cosmic rays presents a challenging task. Specialized shielding systems designed for protection from cosmic rays do not significantly reduce the energy relaxation rate of the SQC. The authors in¹⁴⁰ suggest, that the placement of a dilution refrigerator in a deep underground location and in a room well protected from electromagnetic radiation may be able to accomplish this task.

This method is applicable only if there is a calibrated radiation source. Otherwise, it will be challenging to separate the contributions from quasi-equilibrium quasiparticles and other mechanisms, for example, strongly coupled TLS.

D. Quasiparticles tunneling rate (Γ_{QP})

As far as the quasiparticles generation is associated with the incident radiation^{33–35}, the value of the quasiparticles tunneling rate through a Josephson junction can be an indicator of how much radiation penetrates into the space surrounding the qubit. The main parameter used in this method is the charge parity lifetime (T_P), which can then be converted into a quasiparticle tunneling rate. Measuring the quasiparticle tunneling rate can be done by mapping the charge parity (P) onto the quantum system state¹⁷³, or directly from the dispersive shift of the resonator¹⁶⁷.

Using this method, several experiments were done^{85,174,175}. Authors of¹⁷⁴ have carried out research of various shielding systems and their comparison. As a result, it was demonstrated that different shielding systems may not exhibit significant variations in qubit lifetimes of up to 400 μs in the presence of the mixing chamber shield, but they do influence the tunneling rate of quasiparticles. Thus, the tunneling rate of quasiparticles is a more sensitive parameter than qubit relaxation rate for shielding efficiency evaluation. In¹⁷⁵ it was tested how the length of the IR filter affect the quasiparticles tunneling rate. It was found that the first 0.9 cm of the IR filter is the most effective for quasiparticle tunneling rate decreasing. In⁸⁵ it was shown that considered method is applicable for definition of IR filter position in cryogenic setup. Author of⁸⁵ approve that IR filter is better to mount as closer as possible to SQC.

All of these results demonstrate that quasiparticle tunneling rate can be used as universal parameter for effectiveness eval-

uation of both shielding system and filtering of microwave lines. We recommend using the charge parity measurement method as the most accurate one.

E. Other methods of shielding system effectiveness evaluation

An alternative way for shielding effectiveness estimation can be done by using detectors designated for each type of parasitic factor, e.g., IR radiation and stray electromagnetic fields. Such an approach could allow us to estimate the effectiveness of the shielding constituent parts. Unfortunately, it is not always possible to fabricate a special device and set up a measurement procedure. Moreover, IR detectors are typically fabricated not from the same materials as SQC, that cause additional technological disbursements. Another way for shielding testing is using SQUIDs for electromagnetic noise detection. It can be a SQUID magnetometer^{176,177} or the qubits themselves¹⁷⁸. However, it is out of the scope of this paper.

V. SUMMARY AND OUTLOOK

In this review, we have described the requirements for the shielding system to protect the SQC from external IR radiation and stray electromagnetic fields. We have considered a variety of existing shielding systems and compare them to our requirements. We have also considered different techniques for shielding system effectiveness evaluation.

A. Recommendations for shielding and filtering

The conclusions from the previous paragraphs are that there are no specific recommendations for shielding superconducting quantum circuits. Nevertheless, such recommendations can be made using theories of electromagnetic shielding and heat transfer by radiation. Based on these theories and the modelling results, it is possible to identify the most effective shielding system. As a result, the following recommendations were formulated:

1. The shielding system should consist of at least three shields: an IR shield, a superconducting shield, and a μ -metal one.
2. All the shields should be light-tight. It is necessary to prevent the penetration of IR radiation inside the shield. For superconducting and μ -metal shields, it allows for the magnetic field equalising in the entire shield volume.
3. In order to create a more compact shield, shielding functions may be combined. Specifically, an IR shield can be combined with a superconducting one by depositing a superconducting layer on a copper base.

4. For creating IR shielding with a high efficiency, it should consist of a base with a high thermal conductivity (copper or superconductor coated copper). The shield should have a light-tight lid sealed by the indium wire. The inner surface of IR shield should be coated by the mixture of absorbing coating composed of Stycast epoxy and SiC particles of about 1 mm. The shield should be placed as close to the SQC as possible.
5. For protection from magnetic fields, it is recommended to use a combination of two shields, i.e. an internal superconducting shield and an external μ -metal shield. Such shields arrangement allows for the lowest possible level of stray magnetic field inside the shields.
6. Superconducting shields can be implemented in two ways. The first method involves a single-layer superconducting aluminum shield following after IR shield. The second method utilizes a combined shield consisting of a superconducting layer on a copper light-tight shield coated by an absorbing material and surrounding the sample holder.
7. The μ -metal shield should be made of a material with a high relative magnetic permeability (100,000 or more), placed right after the IR shield and the superconducting one.
8. The placement of magnetic components of the cryogenic setup (e.g., isolators, circulators) should be done outside the shielding. A special design features, such as waveguides on the lid, can additionally reduce the influence of the magnetic field on the quantum circuit. Besides, placing the dilution refrigerator inside a shielded laboratory or in a deep underground location can reduce the influence of the cosmic rays.
9. The sample holder serves as the first layer of shielding. The recommendations for its fabrication are similar to those for IR shielding (see point 4 of current recommendations list). The design of the sample holder should be selected based on the SQC design and the wiring method to the cryogenic setup.
10. The best protection of the superconducting quantum circuit from stray electromagnetic fields and IR radiation can be achieved by combining the shielding and microwave filters. To effectively filter the input line, both RF and MW filters and IR ones should be used, specifically BPF+IR or HPF+LPF+IR. Eccosorb CR-110 epoxy should be chosen as a filler for the IR filters. The IR filters should be placed inside the shield thermalized on the lower stage of dilution refrigerator, while the RF and MW filters don't have such requirement. The output readout line should be filtered in the same manner as the input one. For drive and flux lines, LPF+IR should be used, because it protects from IR radiation propagating along the microwave lines.

All the recommendations given enable the creation of a high efficient and compact shielding system that protects the SQC from stray electromagnetic fields and IR radiation.

B. Method for shielding testing

The shielding system effectiveness can be most accurately evaluated by the method based on the measurement of the quasiparticle tunneling rate. This method provides a higher level of resolution compared to the other methods and allows for choosing different shielding and filtering systems.

VI. REFERENCES

- ¹Y. Nakamura, Y. A. Pashkin, and J. S. Tsai, "Coherent control of macroscopic quantum states in a single-cooper-pair box," *Nature* **398**, 786–788 (1999).
- ²A. Blais, A. L. Grimsmo, S. M. Girvin, and A. Wallraff, "Circuit quantum electrodynamics," *Rev. Mod. Phys.* **93**, 025005 (2021).
- ³P. Krantz, M. Kjaergaard, F. Yan, T. P. Orlando, S. Gustavsson, and W. D. Oliver, "A quantum engineer's guide to superconducting qubits," *Applied Physics Reviews* **6**, 021318 (2019), https://pubs.aip.org/aip/apr/article-pdf/doi/10.1063/1.5089550/16667201/021318_1_online.pdf.
- ⁴M. Kjaergaard, M. E. Schwartz, J. Braumüller, P. Krantz, J. I.-J. Wang, S. Gustavsson, and W. D. Oliver, "Superconducting qubits: Current state of play," *Annual Review of Condensed Matter Physics* **11**, 369–395 (2020).
- ⁵F. Arute, K. Arya, R. Babbush, D. Bacon, J. Bardin, R. Barends, R. Biswas, S. Boixo, F. Brandao, D. Buell, B. Burkett, Y. Chen, J. Chen, B. Chiaro, R. Collins, W. Courtney, A. Dunsworth, E. Farhi, B. Foxen, A. Fowler, C. M. Gidney, M. Giustina, R. Graff, K. Guerin, S. Habegger, M. Harrigan, M. Hartmann, A. Ho, M. R. Hoffmann, T. Huang, T. Humble, S. Isakov, E. Jeffrey, Z. Jiang, D. Kafri, K. Kechedzhi, J. Kelly, P. Klimov, S. Knysh, A. Korotkov, F. Kostritsa, D. Landhuis, M. Lindmark, E. Lucero, D. Lyakh, S. Mandrà, J. R. McClean, M. McEwen, A. Megrant, X. Mi, K. Michielsen, M. Mohseni, J. Mutus, O. Naaman, M. Neeley, C. Neill, M. Y. Niu, E. Ostby, A. Petukhov, J. Platt, C. Quintana, E. G. Rieffel, P. Roushan, N. Rubin, D. Sank, K. J. Satzinger, V. Smelyanskiy, K. J. Sung, M. Trevithick, A. Vainsencher, B. Villalonga, T. White, Z. J. Yao, P. Yeh, A. Zalcman, H. Neven, and J. Martinis, "Quantum supremacy using a programmable superconducting processor," *Nature* **574**, 505–510 (2019).
- ⁶A. Morvan, B. Villalonga, X. Mi, S. andrà, A. Bengtsson, P. V. Klimov, Z. Chen, S. Hong, C. Erickson, I. K. Drozdov, J. Chau, G. Laun, R. Movassagh, A. Asfaw, L. T. A. N. Brandão, R. Peralta, D. Abanin, R. Acharya, R. Allen, T. I. Andersen, K. Anderson, M. Ansmann, F. Arute, K. Arya, J. Atalaya, J. C. Bardin, A. Bilmes, G. Bortoli, A. Bourassa, J. Bovaird, L. Brill, M. Broughton, B. B. Buckley, D. A. Buell, T. Burger, B. Burkett, N. Bushnell, J. Campero, H.-S. Chang, B. Chiaro, D. Chik, C. Chou, J. Cogan, R. Collins, P. Conner, W. Courtney, A. L. Crook, B. Curtin, D. M. Debroy, A. D. T. Barba, S. Demura, A. D. Paolo, A. Dunsworth, L. Faoro, E. Farhi, R. Fatemi, V. S. Ferreira, L. F. Burgos, E. Forati, A. G. Fowler, B. Foxen, G. Garcia, É. Genois, W. Jiang, C. Gidney, D. Gilboa, M. Giustina, R. Gosula, A. G. Dau, J. A. Gross, S. Habegger, M. C. Hamilton, M. Hansen, M. P. Harrigan, S. D. Harrington, P. Heu, M. R. Hoffmann, T. Huang, A. Huff, W. J. Huggins, L. B. Ioffe, S. V. Isakov, J. Iveland, E. Jeffrey, Z. Jiang, C. Jones, P. Juhas, D. Kafri, T. Khattar, M. Khezri, M. Kieferová, S. Kim, A. Kitaev, A. R. Klotz, A. N. Korotkov, F. Kostritsa, J. M. Kreikebaum, D. Landhuis, P. Laptev, K.-M. Lau, L. Laws, J. Lee, K. W. Lee, Y. D. Lensky, B. J. Lester, A. T. Lill, W. Liu, W. P. Livingston, A. Locharla, F. D. Malone, O. Martin, S. Martin, J. R. McClean, M. McEwen, K. C. Miao, A. Mieszala, S. Montazeri, W. Mruczkiewicz, O. Naaman, M. Neeley, C. Neill, A. Nersisyan, M. Newman, J. H. Ng, A. Nguyen, M. Nguyen, M. Y. Niu, T. E. O'Brien, S. Omonije, A. Opremcak, A. Petukhov, R. Potter, L. P. Pryadko, C. Quintana, D. M. Rhodes, C. Rocque, E. Rosenberg, N. C. Rubin, N. Saei, D. Sank, K. Sankaragomathi, K. J. Satzinger, H. F. Schurkus, C. Schuster, M. J. Shearn, A. Shorter, N. Shutt, V. Shvarts, V. Sivak, J. Skrzynny, W. C. Smith, R. D. Somma, G. Sterling, D. Strain, M. Szalay, D. Thor, A. Torres, G. Vidal, C. V. Heidweiller, T. White, B. W. K. Woo, C. Xing,

- Z. J. Yao, P. Yeh, J. Yoo, G. Young, A. Zalcman, Y. Zhang, N. Zhu, N. Zobrist, E. G. Rieffel, R. Biswas, R. Babbush, D. Bacon, J. Hilton, E. Lucero, H. Neven, A. Megrant, J. Kelly, P. Roushan, I. Aleiner, V. Smelyanskiy, K. Kechedzhi, Y. Chen, and S. Boixo, "Phase transitions in random circuit sampling," *Nature* **634**, 328–333 (2024).
- ⁷R. Acharya, D. A. Abanin, L. Aghababaie-Beni, I. Aleiner, T. I. Andersen, M. Ansmann, F. Arute, K. Arya, A. Asfaw, N. Astrakhantsev, J. Atalaya, R. Babbush, D. Bacon, B. Ballard, J. C. Bardin, J. Bausch, A. Bengtsson, A. Bिल्mes, S. Blackwell, S. Boixo, G. Bortoli, A. Bourassa, J. Bovaird, L. Brill, M. Broughton, D. A. Browne, B. Buchea, B. B. Buckley, D. A. Buell, T. Burger, B. Burkett, N. Bushnell, A. Cabrera, J. Campero, H.-S. Chang, Y. Chen, Z. Chen, B. Chiaro, D. Chik, C. Chou, J. Claes, A. Y. Cleland, J. Cogan, R. Collins, P. Conner, W. Courtney, A. L. Crook, B. Curtin, S. Das, A. Davies, L. De Lorenzo, D. M. Debroy, S. Demura, M. Devoret, A. Di Paolo, P. Donohoe, I. Drozdov, A. Dunsworth, C. Earle, T. Edlich, A. Eickbusch, A. M. Elbag, M. Elzouka, C. Erickson, L. Faoro, V. S. Farhi, Edwardand Ferreira, L. F. Burgos, E. Forati, A. G. Fowler, B. Foxen, S. Ganjam, G. Garcia, R. Gasca, É. Genois, W. Giang, C. Gidney, D. Gilboa, A. G. Gosula, Rajaand Dau, D. Graumann, A. Greene, J. A. Gross, S. Habegger, J. Hall, M. C. Hamilton, M. Hansen, M. P. Harrigan, S. D. Harrington, F. J. H. Heras, S. Heslin, P. Heu, O. Higgott, G. Hill, J. Hilton, G. Holland, S. Hong, H.-Y. Huang, A. Huff, W. J. Huggins, L. B. Ioffe, S. V. Isakov, J. Iveland, E. Jeffrey, Z. Jiang, C. Jones, S. Jordan, C. Joshi, P. Juhas, D. Kafri, H. Kang, A. H. Karamlou, K. Kechedzhi, J. Kelly, T. Khair, T. Khattar, M. Khezri, S. Kim, A. R. Klimov, Paul V. and Klotz, B. Kober, P. Kohli, A. N. Koroikov, F. Kostritsa, R. Kothari, B. Kozlovskii, V. D. Kreikebaum, John Markand Kurilovich, N. Lacroix, D. Landhuis, T. Lange-Dei, B. W. Langley, P. Laptev, K.-M. Lau, L. Le Guevel, J. Ledford, J. Lee, K. Lee, Y. D. Lensky, S. Leon, B. J. Lester, W. Y. Li, Y. Li, A. T. Lill, W. Liu, W. P. Livingston, A. Lochar, E. Lucero, D. Lundahl, A. Lunt, S. Madhuk, F. D. Malone, A. Maloney, S. Mandrà, J. Manyika, L. S. Martin, O. Martin, S. Martin, C. Maxfield, J. R. McClean, M. McEwen, S. Meeks, A. Megrant, X. Mi, K. C. Miao, A. Mieszala, R. Molavi, S. Molina, S. Montazeri, A. Morvan, R. Movassagh, W. Mruczkiewicz, O. Naaman, M. Neeley, C. Neill, A. Nersisyan, H. Neven, M. Newman, J. H. Ng, A. Nguyen, M. Nguyen, C.-H. Ni, M. Y. Niu, T. E. O'Brien, W. D. Oliver, A. Opremcak, K. Ottosson, A. Petukhov, A. Pizzuto, J. Platt, R. Potter, O. Pritchard, L. P. Pryadko, C. Quintana, G. Ramachandran, M. J. Reagor, J. Redding, D. M. Rhodes, G. Roberts, E. Rosenberg, E. Rosenfeld, P. Roushan, N. C. Rubin, N. Saei, D. Sank, K. Sankaragomathi, K. J. Satzinger, H. F. Schurkus, C. Schuster, A. W. Senior, M. J. Shearn, A. Shorter, N. Shutty, V. Shvarts, S. Singh, V. Sivak, J. Skrzynski, S. Small, V. Smelyanskiy, W. C. Smith, R. D. Somma, S. Springer, G. Sterling, D. Strain, J. Suchard, A. Szasz, A. Szein, D. Thor, A. Torres, M. M. Torunbalci, A. Vaishnav, J. Vargas, S. Vdovichev, G. Vidal, B. Villalonga, C. V. Heidweiller, S. Waltman, S. X. Wang, B. Ware, K. Weber, T. Weidel, T. White, K. Wong, B. W. K. Woo, C. Xing, Z. J. Yao, P. Yeh, B. Ying, J. Yoo, N. Yosri, G. Young, A. Zalcman, Y. Zhang, N. Zhu, N. Zobrist, G. Q. AI, and Collaborators, "Quantum error correction below the surface code threshold," *Nature* **638**, 920–926 (2025).
- ⁸D. Gao, D. Fan, C. Zha, J. Bei, G. Cai, J. Cai, S. Cao, F. Chen, J. Chen, K. Chen, X. Chen, X. Chen, Z. Chen, Z. Chen, Z. Chen, W. Chu, H. Deng, Z. Deng, P. Ding, X. Ding, Z. Ding, S. Dong, Y. Dong, B. Fan, Y. Fu, S. Gao, L. Ge, M. Gong, J. Gui, C. Guo, S. Guo, X. Guo, L. Han, T. He, L. Hong, Y. Hu, H.-L. Huang, Y.-H. Huo, T. Jiang, Z. Jiang, H. Jin, Y. Leng, D. Li, D. Li, F. Li, J. Li, J. Li, J. Li, J. Li, N. Li, S. Li, W. Li, Y. Li, Y. Li, F. Liang, X. Liang, N. Liao, J. Lin, W. Lin, D. Liu, H. Liu, M. Liu, X. Liu, X. Liu, Y. Liu, H. Lou, Y. Ma, L. Meng, H. Mou, K. Nan, B. Nie, M. Nie, J. Ning, L. Niu, W. Peng, H. Qian, H. Rong, T. Rong, H. Shen, Q. Shen, H. Su, F. Su, C. Sun, L. Sun, T. Sun, Y. Sun, Y. Tan, J. Tan, L. Tang, W. Tu, C. Wan, J. Wang, B. Wang, C. Wang, C. Wang, C. Wang, J. Wang, L. Wang, R. Wang, S. Wang, X. Wang, X. Wang, X. Wang, Y. Wang, Z. Wei, J. Wei, D. Wu, G. Wu, J. Wu, S. Wu, Y. Wu, S. Xie, L. Xin, Y. Xu, C. Xue, K. Yan, W. Yang, X. Yang, Y. Yang, Y. Ye, Z. Ye, C. Ying, J. Yu, Q. Yu, W. Yu, X. Zeng, S. Zhan, F. Zhang, H. Zhang, K. Zhang, P. Zhang, W. Zhang, Y. Zhang, Y. Zhang, L. Zhang, G. Zhao, P. Zhao, X. Zhao, X. Zhao, Y. Zhao, Z. Zhao, L. Zheng, F. Zhou, L. Zhou, N. Zhou, N. Zhou, S. Zhou, S. Zhou, Z. Zhou, C. Zhu, Q. Zhu, G. Zou, H. Zou, Q. Zhang, C.-Y. Lu, C.-Z. Peng, X. Zhu, and J.-W. Pan, "Establishing a new benchmark in quantum computational advantage with 105-qubit zuhongzhi 3.0 processor," *Phys. Rev. Lett.* **134**, 090601 (2025).
- ⁹Y. Kim, A. Eddins, S. Anand, K. X. Wei, E. van den Berg, S. Rosenblatt, H. Nayfeh, Y. Wu, M. Zaletel, K. Temme, and A. Kandala, "Evidence for the utility of quantum computing before fault tolerance," *Nature* **618**, 500–505 (2023).
- ¹⁰J. Bylander, S. Gustavsson, F. Yan, F. Yoshihara, K. Harrabi, G. Fitch, D. G. Cory, Y. Nakamura, J.-S. Tsai, and W. D. Oliver, "Noise spectroscopy through dynamical decoupling with a superconducting flux qubit," *Nature Physics* **7**, 565–570 (2011).
- ¹¹R. H. Koch, D. P. DiVincenzo, and J. Clarke, "Model for $1/f$ flux noise in squids and qubits," *Phys. Rev. Lett.* **98**, 267003 (2007).
- ¹²F. Yan, J. Bylander, S. Gustavsson, F. Yoshihara, K. Harrabi, D. G. Cory, T. P. Orlando, Y. Nakamura, J.-S. Tsai, and W. D. Oliver, "Spectroscopy of low-frequency noise and its temperature dependence in a superconducting qubit," *Phys. Rev. B* **85**, 174521 (2012).
- ¹³R. C. Bialczak, R. McDermott, M. Ansmann, M. Hofheinz, N. Katz, E. Lucero, M. Neeley, A. D. O'Connell, H. Wang, A. N. Cleland, and J. M. Martinis, " $1/f$ flux noise in josephson phase qubits," *Phys. Rev. Lett.* **99**, 187006 (2007).
- ¹⁴D. I. Schuster, A. Wallraff, A. Blais, L. Frunzio, R.-S. Huang, J. Majer, S. M. Girvin, and R. J. Schoelkopf, "ac stark shift and dephasing of a superconducting qubit strongly coupled to a cavity field," *Phys. Rev. Lett.* **94**, 123602 (2005).
- ¹⁵S. Ganjam, Y. Wang, Y. Lu, A. Banerjee, C. U. Lei, L. Krayzman, K. Kisslinger, C. Zhou, R. Li, Y. Jia, M. Liu, L. Frunzio, and R. J. Schoelkopf, "Surpassing millisecond coherence in on chip superconducting quantum memories by optimizing materials and circuit design," *Nature Communications* **15**, 3687 (2024).
- ¹⁶X. Pan, Y. Zhou, H. Yuan, L. Nie, W. Wei, L. Zhang, J. Li, S. Liu, Z. H. Jiang, G. Catelani, L. Hu, F. Yan, and D. Yu, "Engineering superconducting qubits to reduce quasiparticles and charge noise," *Nature Communications* **13**, 7196 (2022).
- ¹⁷S. Kim, H. Terai, T. Yamashita, W. Qiu, T. Fuse, F. Yoshihara, S. Ashhab, K. Inomata, and K. Semba, "Enhanced coherence of all-nitride superconducting qubits epitaxially grown on silicon substrate," *Communications Materials* **2**, 98 (2021).
- ¹⁸A. P. M. Place, L. V. H. Rodgers, P. Mundada, B. M. Smitham, M. Fitzpatrick, Z. Leng, A. Premkumar, J. Bryon, A. Vrajitoarea, S. Sussman, G. Cheng, T. Madhavan, H. K. Babla, X. H. Le, Y. Gang, B. Jäck, A. Gyenis, N. Yao, R. J. Cava, N. P. de Leon, and A. A. Houck, "New material platform for superconducting transmon qubits with coherence times exceeding 0.3 milliseconds," *Nature Communications* **12** (2021), 10.1038/s41467-021-22030-5.
- ¹⁹W. D. Oliver and P. B. Welander, "Materials in superconducting quantum bits," *MRS Bulletin* **38**, 816–825 (2013).
- ²⁰A. A. Pishchikova, N. S. Smirnov, D. A. Ezenkova, E. A. Krivko, E. V. Zikiy, D. O. Moskalev, A. I. Ivanov, N. D. Korshakov, and I. A. Rodionov, "Improving josephson junction reproducibility for superconducting quantum circuits: junction area fluctuation," *Scientific Reports* **13**, 6772 (2023).
- ²¹D. O. Moskalev, E. V. Zikiy, A. A. Pishchikova, D. A. Ezenkova, N. S. Smirnov, A. I. Ivanov, N. D. Korshakov, and I. A. Rodionov, "Optimization of shadow evaporation and oxidation for reproducible quantum josephson junction circuits," *Scientific Reports* **13**, 4174 (2023).
- ²²G. Ithier, E. Collin, P. Joyez, P. J. Meeson, D. Vion, D. Esteve, F. Chiarello, A. Shnirman, Y. Makhlin, J. Schrieffer, and G. Schön, "Decoherence in a superconducting quantum bit circuit," *Phys. Rev. B* **72**, 134519 (2005).
- ²³A. D. Córcoles, J. M. Chow, J. M. Gambetta, C. Rigetti, J. R. Rozen, G. A. Keefe, M. Beth Rothwell, M. B. Ketchen, and M. Steffen, "Protecting superconducting qubits from radiation," *Applied Physics Letters* **99**, 181906 (2011), https://pubs.aip.org/aip/apl/article-pdf/doi/10.1063/1.3658630/16731205/181906_1_online.pdf.
- ²⁴V. Zaretsky, S. Novikov, B. Suri, Z. Kim, F. Wellstood, and B. Palmer, "Decoherence in a pair of long-lived cooper-pair boxes," *Journal of Applied Physics* **114** (2013).
- ²⁵P. J. de Visser, J. J. A. Baselmans, P. Diener, S. J. C. Yates, A. Endo, and T. M. Klapwijk, "Number fluctuations of sparse quasiparticles in a superconductor," *Phys. Rev. Lett.* **106**, 167004 (2011).

- ²⁶G. Calusine, A. Melville, W. Woods, R. Das, C. Stull, V. Bolkhovskiy, D. Braje, D. Hover, D. K. Kim, X. Miloshi, D. Rosenberg, A. Sevi, J. L. Yoder, E. Dauler, and W. D. Oliver, “Analysis and mitigation of interface losses in trenched superconducting coplanar waveguide resonators,” *Applied Physics Letters* **112**, 062601 (2018), https://pubs.aip.org/apl/article-pdf/doi/10.1063/1.5006888/13301762/062601_1_online.pdf.
- ²⁷C. Wang, C. Axline, Y. Gao, T. Brecht, Y. Chu, L. Frunzio, M. Devoret, and R. Schoelkopf, “Surface participation and dielectric loss in superconducting qubits,” *APPLIED PHYSICS LETTERS* **107**, 162601 (2015).
- ²⁸W. Woods, G. Calusine, A. Melville, A. Sevi, E. Golden, D. Kim, D. Rosenberg, J. Yoder, and W. Oliver, “Determining interface dielectric losses in superconducting coplanar-waveguide resonators,” *Physical Review Applied* **12** (2019), 10.1103/physrevapplied.12.014012.
- ²⁹E. M. Purcell, “Spontaneous Emission Probabilities at Radio Frequencies,” *Physical Review* **69**, 681 (1946).
- ³⁰J. M. Martinis, “Saving superconducting quantum processors from decay and correlated errors generated by gamma and cosmic rays,” *npj Quantum Information* **7**, 90 (2021).
- ³¹M. H. Devoret, A. Wallraff, and J. M. Martinis, “Superconducting qubits: A short review,” (2004), [arXiv:cond-mat/0411174](https://arxiv.org/abs/cond-mat/0411174) [cond-mat.mes-hall].
- ³²S. Krinner, S. Storz, P. Kurpiers, P. Magnard, J. Heinsoo, R. Keller, J. Lütolf, C. Eichler, and A. Wallraff, “Engineering cryogenic setups for 100-qubit scale superconducting circuit systems,” *EPJ Quantum Technology* **6**, 2 (2019).
- ³³J. M. Martinis, M. Ansmann, and J. Aumentado, “Energy decay in superconducting josephson-junction qubits from nonequilibrium quasiparticle excitations,” *Phys. Rev. Lett.* **103**, 097002 (2009).
- ³⁴G. Catelani, R. J. Schoelkopf, M. H. Devoret, and L. I. Glazman, “Relaxation and frequency shifts induced by quasiparticles in superconducting qubits,” *Phys. Rev. B* **84**, 064517 (2011).
- ³⁵G. Catelani, S. E. Nigg, S. M. Girvin, R. J. Schoelkopf, and L. I. Glazman, “Decoherence of superconducting qubits caused by quasiparticle tunneling,” *Phys. Rev. B* **86**, 184514 (2012).
- ³⁶A. Eddins, S. Schreppler, D. M. Toyli, L. S. Martin, S. Hacohe-Gourgy, L. C. G. Govia, H. Ribeiro, A. A. Clerk, and I. Siddiqi, “Stroboscopic qubit measurement with squeezed illumination,” *Phys. Rev. Lett.* **120**, 040505 (2018).
- ³⁷J. J. Burnett, A. Bengtsson, M. Scigliuzzo, D. Niepce, M. Kudra, P. Delsing, and J. Bylander, “Decoherence benchmarking of superconducting qubits,” *npj Quantum Information* **5** (2019), 10.1038/s41534-019-0168-5.
- ³⁸M. E. Schwartz, *Engineering Dissipation to Generate Entanglement Between Remote Superconducting Quantum Bits*, Ph.D. thesis, University of California in Berkeley (2016).
- ³⁹A. Premkumar, C. Weiland, S. Hwang, B. Jäck, A. P. M. Place, I. Waluyo, A. Hunt, V. Bisogni, J. Pellicciari, A. Barbour, M. S. Miller, P. Russo, F. Camino, K. Kisslinger, X. Tong, M. S. Hybertsen, A. A. Houck, and I. Jarrige, “Microscopic relaxation channels in materials for superconducting qubits,” *Communications Materials* **2**, 72 (2021).
- ⁴⁰F. Yan, S. Gustavsson, A. Kamal, J. Birenbaum, A. P. Sears, D. Hover, T. J. Gudmundsen, D. Rosenberg, G. Samach, S. Weber, J. L. Yoder, T. P. Orlando, J. Clarke, A. J. Kerman, and W. D. Oliver, “The flux qubit revisited to enhance coherence and reproducibility,” *Nature Communications* **7** (2016), 10.1038/ncomms12964.
- ⁴¹V. Schmitt, *Design, fabrication and test of a four superconducting quantum-bit processor*, Ph.D. thesis, Sorbonne University Pierre and Marie Curie Campus (2015).
- ⁴²J. Burnett, *High Precision readout of superconducting resonators for analysis of slow noise processes*, Ph.D. thesis, Royal Holloway University of London (2013).
- ⁴³A. D. Córcoles, E. Magesan, S. J. Srinivasan, A. W. Cross, M. Steffen, J. M. Gambetta, and J. M. Chow, “Demonstration of a quantum error detection code using a square lattice of four superconducting qubits,” *Nature Communications* **6**, 6979 (2015).
- ⁴⁴R. Barends, J. Wenner, M. Lenander, Y. Chen, R. Bialczak, J. Kelly, E. Lucero, P. O’Malley, M. Mariantoni, D. Sank, *et al.*, “Minimizing quasiparticle generation from stray infrared light in superconducting quantum circuits,” *APPLIED PHYSICS LETTERS* **99**, 113507 (2011).
- ⁴⁵S. M. Smith, “Specular reflectance of optical-black coatings in the far infrared,” *Appl. Opt.* **23**, 2311–2326 (1984).
- ⁴⁶J. W. Ekin, “Introduction to Measurement Cryostats and Cooling Methods,” in *Experimental Techniques for Low-Temperature Measurements: Cryostat Design, Material Properties and Superconductor Critical-Current Testing* (Oxford University Press, 2006) https://academic.oup.com/book/0/chapter/270047394/chapter-ag-pdf/44539367/book_32506_section_270047394.ag.pdf.
- ⁴⁷S. Bailly, “Gold - physical, mechanical, thermal, and electrical properties,” Accessed on July 22, 2024.
- ⁴⁸M. shield Corp., “Mu-metal: Technical data,” Accessed on July 22, 2024.
- ⁴⁹K. S. Chou, *Teleported operations between logical qubits in circuit quantum electrodynamics*, Ph.D. thesis, Yale University (2018).
- ⁵⁰C. Dickel, J. J. Wesdorp, N. K. Langford, S. Peiter, R. Sagastizabal, A. Bruno, B. Criger, F. Motzoi, and L. DiCarlo, “Chip-to-chip entanglement of transmon qubits using engineered measurement fields,” *Phys. Rev. B* **97**, 064508 (2018).
- ⁵¹I. M. Pop, K. Geerlings, G. Catelani, R. J. Schoelkopf, L. I. Glazman, and M. H. Devoret, “Coherent suppression of electromagnetic dissipation due to superconducting quasiparticles,” *Nature* **508**, 369–372 (2014).
- ⁵²J. T. Monroe, N. Yünger Halpern, T. Lee, and K. W. Murch, “Weak measurement of a superconducting qubit reconciles incompatible operators,” *Phys. Rev. Lett.* **126**, 100403 (2021).
- ⁵³Here and further, the estimate of mention frequency of a certain parameter is given from the total number of works where this parameter is found.
- ⁵⁴F. Henriques, F. Valenti, T. Charpentier, M. Lagoon, C. Gouriou, M. Martínez, L. Cardani, M. Vignati, L. Grünhaupt, D. Gusenkova, *et al.*, “Phonon traps reduce the quasiparticle density in superconducting circuits,” *Applied physics letters* **115** (2019).
- ⁵⁵A. Gienis, P. S. Mundada, A. Di Paolo, T. M. Hazard, X. You, D. I. Schuster, J. Koch, A. Blais, and A. A. Houck, “Experimental realization of a protected superconducting circuit derived from the 0– π qubit,” *PRX Quantum* **2**, 010339 (2021).
- ⁵⁶T. M. Hazard, *Improving Quantum Hardware: Building New Superconducting Qubits and Couplers*, Ph.D. thesis, Princeton University (2019).
- ⁵⁷W. C. Smith, *Design of Protected Superconducting Qubits*, Ph.D. thesis, Yale University (2019).
- ⁵⁸S. Poletto, J. M. Gambetta, S. T. Merkel, J. A. Smolin, J. M. Chow, A. D. Córcoles, G. A. Keefe, M. B. Rothwell, J. R. Rozen, D. W. Abraham, C. Rigetti, and M. Steffen, “Entanglement of two superconducting qubits in a waveguide cavity via monochromatic two-photon excitation,” *Phys. Rev. Lett.* **109**, 240505 (2012).
- ⁵⁹M. A. Beck, *Hybrid superconducting quantum computing architectures*, Ph.D. thesis, University of Wisconsin–Madison (2018).
- ⁶⁰Y. Wu, W.-S. Bao, S. Cao, F. Chen, M.-C. Chen, X. Chen, T.-H. Chung, H. Deng, Y. Du, D. Fan, M. Gong, C. Guo, C. Guo, S. Guo, L. Han, L. Hong, H.-L. Huang, Y.-H. Huo, L. Li, N. Li, S. Li, Y. Li, F. Liang, C. Lin, J. Lin, H. Qian, D. Qiao, H. Rong, H. Su, L. Sun, L. Wang, S. Wang, D. Wu, Y. Xu, K. Yan, W. Yang, Y. Yang, Y. Ye, J. Yin, C. Ying, J. Yu, C. Zha, C. Zhang, H. Zhang, K. Zhang, Y. Zhang, H. Zhao, Y. Zhao, L. Zhou, Q. Zhu, C.-Y. Lu, C.-Z. Peng, X. Zhu, and J.-W. Pan, “Strong quantum computational advantage using a superconducting quantum processor,” *Phys. Rev. Lett.* **127**, 180501 (2021).
- ⁶¹B. Ann, *Tunable quantum interfaces between superconducting qubits and microwave photons induced by extreme driving*, Ph.D. thesis, Delft University of Technology (2021).
- ⁶²I. Chiorescu, Y. Nakamura, C. J. P. M. Harmans, and J. E. Mooij, “Coherent quantum dynamics of a superconducting flux qubit,” *Science* **299**, 1869–1871 (2003).
- ⁶³R. Dhuley, “Pressed copper and gold-plated copper contacts at low temperatures – a review of thermal contact resistance,” *Cryogenics* **101**, 111–124 (2019).
- ⁶⁴E. Bründermann and H.-W. Hubers, *Terahertz Techniques*, Springer Series in Optical Sciences (Springer Berlin Heidelberg, Heidelberg, Berlin, 2012).
- ⁶⁵J. Howell, M. Menguc, and R. Siegel, *Thermal Radiation Heat Transfer, 5th Edition* (CRC Press, 2010).
- ⁶⁶L. Grünhaupt, U. von Lüpke, D. Gusenkova, S. T. Skacel, N. Maleeva, S. Schlör, A. Bilmes, H. Rotzinger, A. V. Ustinov, M. Weides, and I. M. Pop, “An argon ion beam milling process for native alox layers enabling coherent superconducting contacts,” *Applied Physics Letters* **111** (2017), 10.1063/1.4990491.

- ⁶⁷N. Maleeva, L. Grünhaupt, T. Klein, F. Levy-Bertrand, O. Dupre, M. Calvo, F. Valenti, P. Winkel, F. Friedrich, W. Wernsdorfer, A. V. Ustinov, H. Rotzinger, A. Monfardini, M. V. Fistul, and I. M. Pop, "Circuit quantum electrodynamics of granular aluminum resonators," *Nature Communications* **9** (2018), 10.1038/s41467-018-06386-9.
- ⁶⁸X. Y. Jin, A. Kamal, A. P. Sears, T. Gudmundsen, D. Hover, J. Milosli, R. Slattery, F. Yan, J. Yoder, T. P. Orlando, S. Gustavsson, and W. D. Oliver, "Thermal and residual excited-state population in a 3d transmon qubit," *Phys. Rev. Lett.* **114**, 240501 (2015).
- ⁶⁹Z. Wang, S. Shankar, Z. Mineev, P. Campagne-Ibarcq, A. Narla, and M. Devoret, "Cavity attenuators for superconducting qubits," *Phys. Rev. Appl.* **11**, 014031 (2019).
- ⁷⁰G. Zhang, *Tunable Coupling and Its Applications in Circuit Quantum Electrodynamics*, Ph.D. thesis, Princeton University (2018).
- ⁷¹S. Srinivasan, *Tunable Coupling Circuit Quantum Electrodynamics*, Ph.D. thesis, Princeton University (2013).
- ⁷²J. M. Chow, J. M. Gambetta, E. Magesan, D. W. Abraham, A. W. Cross, B. R. Johnson, N. A. Masluk, C. A. Ryan, J. A. Smolin, S. J. Srinivasan, and M. Steffen, "Implementing a strand of a scalable fault-tolerant quantum computing fabric," *Nature Communications* **5**, 4015 (2014).
- ⁷³Y. Liu, *Reservoir engineering in circuit quantum electrodynamics*, Ph.D. thesis, Princeton University (2016).
- ⁷⁴J. G. Kroll, *Magnetic field compatible hybrid circuit quantum electrodynamics*, Ph.D. thesis, Delft University of Technology (2019).
- ⁷⁵C. Rigetti, J. M. Gambetta, S. Poletto, B. L. T. Plourde, J. M. Chow, A. D. Córcoles, J. A. Smolin, S. T. Merkel, J. R. Rozen, G. A. Keefe, M. B. Rothwell, M. B. Ketchen, and M. Steffen, "Superconducting qubit in a waveguide cavity with a coherence time approaching 0.1 ms," *Phys. Rev. B* **86**, 100506 (2012).
- ⁷⁶W. Uilhoorn, *Hybrid Josephson junction-based quantum devices in magnetic field*, Ph.D. thesis, Delft University of Technology (2021).
- ⁷⁷Y. Liu, S. J. Srinivasan, D. Hover, S. Zhu, R. McDermott, and A. A. Houck, "High fidelity readout of a transmon qubit using a superconducting low-inductance undulatory galvanometer microwave amplifier," *New Journal of Physics* **16**, 113008 (2014).
- ⁷⁸I. Laird Technologies, "Eccossorb crs. two-part castable silicone load absorber," Accessed on March 21, 2025.
- ⁷⁹A. Narla, *Flying Qubit Operations in Superconducting Circuits*, Ph.D. thesis, Yale University (2017).
- ⁸⁰D. J. Hover, *Dispersive Readout of a Superconducting Qubit Using a SLUG Amplifier*, Ph.D. thesis, University of Wisconsin-Madison (2013).
- ⁸¹K. L. Geerlings, *Improving Coherence of Superconducting Qubits and Resonators*, Ph.D. thesis, Yale University (2013).
- ⁸²J. R. Lane, D. Tan, N. R. Beysengulov, K. Nasyedkin, E. Brook, L. Zhang, T. Stefanski, H. Byeon, K. W. Murch, and J. Pollanen, "Integrating superfluids with superconducting qubit systems," *Phys. Rev. A* **101**, 012336 (2020).
- ⁸³A. Megrant, C. Neill, R. Barends, B. Chiaro, Y. Chen, L. Feigl, J. Kelly, E. Lucero, M. Mariantoni, P. O'Malley, *et al.*, "Planar superconducting resonators with internal quality factors above one million," *Applied Physics Letters* **100**, 113510 (2012).
- ⁸⁴P. M. Harrington, *Measurement, Dissipation, and Quantum Control with Superconducting Circuits*, Ph.D. thesis, Washington University (2020).
- ⁸⁵K. Serniak, *Nonequilibrium Quasiparticles in Superconducting Qubits*, Ph.D. thesis, Yale University (2019).
- ⁸⁶E. Buks, P. Brookes, E. Ginossar, C. Deng, J.-L. F. X. Orgiazzi, M. Otto, and A. Lupascu, "Driving-induced resonance narrowing in a strongly coupled cavity-qubit system," *Phys. Rev. A* **102**, 043716 (2020).
- ⁸⁷M. Scigliuzzo, L. E. Bruhat, A. Bengtsson, J. J. Burnett, A. F. Roudsari, and P. Delsing, "Phononic loss in superconducting resonators on piezoelectric substrates," *New Journal of Physics* **22**, 053027 (2020).
- ⁸⁸A. Eddins, J. M. Kreikebaum, D. M. Toyli, E. M. Levenson-Falk, A. Dove, W. P. Livingston, B. A. Levitan, L. C. G. Govia, A. A. Clerk, and I. Siddiqi, "High-efficiency measurement of an artificial atom embedded in a parametric amplifier," *Phys. Rev. X* **9**, 011004 (2019).
- ⁸⁹D. L. Underwood, *Microwave Cavity Lattices for Quantum Simulation with Photons*, Ph.D. thesis, Princeton University (2015).
- ⁹⁰W. Cai, J. Han, F. Mei, Y. Xu, Y. Ma, X. Li, H. Wang, Y. P. Song, Z.-Y. Xue, Z.-q. Yin, S. Jia, and L. Sun, "Observation of topological magnon insulator states in a superconducting circuit," *Phys. Rev. Lett.* **123**, 080501 (2019).
- ⁹¹L. D. Burkhardt, J. D. Teoh, Y. Zhang, C. J. Axline, L. Frunzio, M. Devoret, L. Jiang, S. Girvin, and R. Schoelkopf, "Error-detected state transfer and entanglement in a superconducting quantum network," *PRX Quantum* **2**, 030321 (2021).
- ⁹²E. Lucero, R. Barends, Y. Chen, J. Kelly, M. Mariantoni, A. Megrant, P. O'Malley, D. Sank, A. Vainsencher, J. Wenner, T. White, Y. Yin, A. N. Cleland, and J. M. Martinis, "Computing prime factors with a josephson phase qubit quantum processor," *Nature Physics* **8**, 719–723 (2012).
- ⁹³S. J. Srinivasan, N. M. Sundaresan, D. Sadri, Y. Liu, J. M. Gambetta, T. Yu, S. M. Girvin, and A. A. Houck, "Time-reversal symmetrization of spontaneous emission for quantum state transfer," *Phys. Rev. A* **89**, 033857 (2014).
- ⁹⁴P. Kumar, S. Sendelbach, M. A. Beck, J. W. Freeland, Z. Wang, H. Wang, C. C. Yu, R. Q. Wu, D. P. Pappas, and R. McDermott, "Origin and reduction of $1/f$ magnetic flux noise in superconducting devices," *Phys. Rev. Appl.* **6**, 041001 (2016).
- ⁹⁵S. M. Anton, C. Müller, J. S. Birenbaum, S. R. O'Kelley, A. D. Fefferman, D. S. Golubev, G. C. Hilton, H.-M. Cho, K. D. Irwin, F. C. Wellstood, G. Schön, A. Shnirman, and J. Clarke, "Pure dephasing in flux qubits due to flux noise with spectral density scaling as $1/f^\alpha$," *Phys. Rev. B* **85**, 224505 (2012).
- ⁹⁶T. Yamamoto, K. Inomata, K. Koshino, P.-M. Billangeon, Y. Nakamura, and J. S. Tsai, "Superconducting flux qubit capacitively coupled to an lc resonator," *New Journal of Physics* **16**, 015017 (2014).
- ⁹⁷B. Lienhard, J. Braumüller, W. Woods, D. Rosenberg, G. Calusine, S. Weber, A. Vepsäläinen, K. O'Brien, T. P. Orlando, S. Gustavsson, and W. D. Oliver, "Microwave packaging for superconducting qubits," in *2019 IEEE MTT-S International Microwave Symposium (IMS)* (IEEE, 2019).
- ⁹⁸M. S. Blok, V. V. Ramasesh, T. Schuster, K. O'Brien, J. M. Kreikebaum, D. Dahlen, A. Morvan, B. Yoshida, N. Y. Yao, and I. Siddiqi, "Quantum information scrambling on a superconducting qutrit processor," *Phys. Rev. X* **11**, 021010 (2021).
- ⁹⁹S. Huang, B. Lienhard, G. Calusine, A. Vepsäläinen, J. Braumüller, D. K. Kim, A. J. Melville, B. M. Niedzielski, J. L. Yoder, B. Kannan, T. P. Orlando, S. Gustavsson, and W. D. Oliver, "Microwave package design for superconducting quantum processors," *PRX Quantum* **2**, 020306 (2021).
- ¹⁰⁰M. V. Moghaddam, C. Chang, I. Nsanzineza, A. Vadiraj, and C. Wilson, "Carbon nanotube-based lossy transmission line filter for superconducting qubit measurements," *Applied Physics Letters* **115**, 213504 (2019).
- ¹⁰¹L. S. Martin, W. P. Livingston, S. Hacohe-Gourgy, H. M. Wiseman, and I. Siddiqi, "Implementation of a canonical phase measurement with quantum feedback," *Nature Physics* **16**, 1046–1049 (2020).
- ¹⁰²J. Monroe, D. Kowsari, K. Zheng, C. Gaikwad, J. Brewster, D. Wisbey, and K. Murch, "Optical direct write of dolan-niemeyer-bridge junctions for transmon qubits," *Applied Physics Letters* **119**, 062601 (2021).
- ¹⁰³S. T. Merkel, J. M. Gambetta, J. A. Smolin, S. Poletto, A. D. Córcoles, B. R. Johnson, C. A. Ryan, and M. Steffen, "Self-consistent quantum process tomography," *Phys. Rev. A* **87**, 062119 (2013).
- ¹⁰⁴K. Serniak, M. Hays, G. de Lange, S. Diamond, S. Shankar, L. D. Burkhardt, L. Frunzio, M. Houzet, and M. H. Devoret, "Hot nonequilibrium quasiparticles in transmon qubits," *Phys. Rev. Lett.* **121**, 157701 (2018).
- ¹⁰⁵P. J. de Visser, *Quasiparticle dynamics in aluminium superconducting microwave resonators*, Ph.D. thesis, Delft University of Technology (2014).
- ¹⁰⁶J.-H. Yeh, J. LeFebvre, S. Premaratne, F. C. Wellstood, and B. S. Palmer, "Microwave attenuators for use with quantum devices below 100 mk," *Journal of Applied Physics* **121**, 224501 (2017), https://pubs.aip.org/aip/jap/article-pdf/doi/10.1063/1.4984894/9220456/224501_1_online.pdf.
- ¹⁰⁷G. Ribeill, *Qubit readout with the josephson photomultiplier*, Ph.D. thesis, University of Wisconsin-Madison (2016).
- ¹⁰⁸J. M. Chow, *Quantum Information Processing with Superconducting Qubits*, Ph.D. thesis, Yale University (2010).
- ¹⁰⁹Z. Chen, *Metrology of Quantum Control and Measurement in Superconducting Qubits*, Ph.D. thesis, University of California in Santa Barbara (2018).
- ¹¹⁰M. D. Reed, *Entanglement and quantum error correction with superconducting qubits*, Ph.D. thesis, Yale University (2013).
- ¹¹¹N. S. Smirnov, E. A. Krivko, A. A. Solovyova, A. I. Ivanov, and I. A. Rodionov, "Wiring surface loss of a superconducting transmon qubit," *Scienc*

- tific Reports **14**, 7326 (2024).
- ¹¹²J. Lisenfeld, A. Bilmes, A. Megrant, R. Barends, J. Kelly, P. Klimov, G. Weiss, J. M. Martinis, and A. V. Ustinov, "Electric field spectroscopy of material defects in transmon qubits," npj Quantum Information **5** (2019), 10.1038/s41534-019-0224-1.
 - ¹¹³A. P. Sears, *Extending Coherence in Superconducting Qubits: from micro-seconds to milliseconds*, Ph.D. thesis, Yale University (2013).
 - ¹¹⁴S. Asaad, C. Dickel, N. K. Langford, S. Poletto, A. Bruno, M. A. Rol, D. Deurloo, and L. DiCarlo, "Independent, extensible control of same-frequency superconducting qubits by selective broadcasting," npj Quantum Information **2** (2016), 10.1038/npjqi.2016.29.
 - ¹¹⁵T. Lanting, A. J. Przybysz, A. Y. Smirnov, F. M. Spedalieri, M. H. Amin, A. J. Berkley, R. Harris, F. Altomare, S. Boixo, P. Bunyk, N. Dickson, C. Enderud, J. P. Hilton, E. Hoskinson, M. W. Johnson, E. Ladizinsky, N. Ladizinsky, R. Neufeld, T. Oh, I. Perminov, C. Rich, M. C. Thom, E. Tolkacheva, S. Uchaikin, A. B. Wilson, and G. Rose, "Entanglement in a quantum annealing processor," Phys. Rev. X **4**, 021041 (2014).
 - ¹¹⁶D. Sullivan, S. Dutta, M. Dreyer, M. Gubrud, A. Roychowdhury, J. Anderson, C. Lobb, and F. Wellstood, "Asymmetric superconducting quantum interference devices for suppression of phase diffusion in small josephson junctions," Journal of Applied Physics **113**, 183905 (2013).
 - ¹¹⁷Y. Liu, *Quantum Feedback Control of Multiple Superconducting Qubits*, Ph.D. thesis, Yale University (2016).
 - ¹¹⁸M. Jerger, *Experiments on superconducting qubits coupled to resonators*, Ph.D. thesis, Karlsruhe Institute of Technology (2013).
 - ¹¹⁹J. M. Kreikebaum, A. Dove, W. Livingston, E. Kim, and I. Siddiqi, "Optimization of infrared and magnetic shielding of superconducting tin and al coplanar microwave resonators," Superconductor Science and Technology **29**, 104002 (2016).
 - ¹²⁰G. Long, *Studies of phenomena arising from the non-linearity of the Josephson junction*, Ph.D. thesis, Royal Holloway University of London (2019).
 - ¹²¹K. W. Murch, S. J. Weber, C. Macklin, and I. Siddiqi, "Observing single quantum trajectories of a superconducting quantum bit," Nature **502**, 211–214 (2013).
 - ¹²²A. Bengtsson, *Quantum information processing with tunable and low-loss superconducting circuits*, Ph.D. thesis, Chalmers University of Technology (2020).
 - ¹²³M. Mirhosseini, A. Sipahigil, M. Kalaei, and O. Painter, "Superconducting qubit to optical photon transduction," Nature **588**, 599–603 (2020).
 - ¹²⁴E. M. L. Jr., *Digital Control of Superconducting Quantum Bits*, Ph.D. thesis, University of Wisconsin–Madison (2018).
 - ¹²⁵Y. Sung, *Non-Gaussian Noise Spectroscopy with Superconducting Qubits*, Ph.D. thesis, Massachusetts Institute of Technology (2018).
 - ¹²⁶N. Roch, M. E. Schwartz, F. Motzoi, C. Macklin, R. Vijay, A. W. Eddins, A. N. Korotkov, K. B. Whaley, M. Sarovar, and I. Siddiqi, "Observation of measurement-induced entanglement and quantum trajectories of remote superconducting qubits," Phys. Rev. Lett. **112**, 170501 (2014).
 - ¹²⁷C. Dickel, *Scalability and modularity for transmon-based quantum processors*, Ph.D. thesis, Delft University of Technology (2018).
 - ¹²⁸S. Shankar, M. Hatridge, Z. Leghtas, K. M. Sliwa, A. Narla, U. Vool, S. M. Girvin, L. Frunzio, M. Mirrahimi, and M. H. Devoret, "Autonomously stabilized entanglement between two superconducting quantum bits," Nature **504**, 419–422 (2013).
 - ¹²⁹Z. Mineev, S. Mundhada, S. Shankar, P. Reinhold, R. Gutiérrez-Jáuregui, R. Schoelkopf, M. Mirrahimi, H. Carmichael, and M. Devoret, "To catch and reverse a quantum jump mid-flight," Nature **570**, 200–204 (2019).
 - ¹³⁰D. Lachance-Quirion, Y. Tabuchi, S. Ishino, A. Noguchi, T. Ishikawa, R. Yamazaki, and Y. Nakamura, "Resolving quanta of collective spin excitations in a millimeter-sized ferromagnet," Science Advances **3**, e1603150 (2017), <https://www.science.org/doi/pdf/10.1126/sciadv.1603150>.
 - ¹³¹M. Kudra, J. Biznárová, A. F. Roudsari, J. Burnett, D. Niepce, S. Gasparinetti, B. Wickman, and P. Delsing, "High quality three-dimensional aluminum microwave cavities," Applied Physics Letters **117**, 070601 (2020).
 - ¹³²M. J. Reagor, *Superconducting Cavities for Circuit Quantum Electrodynamics*, Ph.D. thesis, Yale University (2015).
 - ¹³³Amuncal, "Magnetic shielding materials," Accessed on July 23, 2024.
 - ¹³⁴Aperam, "Cryophy," Accessed on July 23, 2024.
 - ¹³⁵V. C. Le, M. Slodička, and K. Van Bockstal, "A time discrete scheme for an electromagnetic contact problem with moving conductor," Appl. Math. Comput. **404** (2021), 10.1016/j.amc.2021.125997.
 - ¹³⁶A. M. Opremcak, *Qubit State Measurement Using a Microwave Photon Counter*, Ph.D. thesis, University of Wisconsin-Madison (2020).
 - ¹³⁷Y. Y. Gao, *Multi-Cavity Operations in Circuit Quantum Electrodynamics*, Ph.D. thesis, Yale University (2018).
 - ¹³⁸S. Mundhada, *Hardware-Efficient Autonomous Quantum Error Correction*, Ph.D. thesis, Yale University (2020).
 - ¹³⁹C. D. Wilen, S. Abdullah, N. A. Kurinsky, C. Stanford, L. Cardani, G. D'Imperio, C. Tomei, L. Faoro, L. B. Ioffe, C. H. Liu, A. Opremcak, B. G. Christensen, J. L. DuBois, and R. McDermott, "Correlated charge noise and relaxation errors in superconducting qubits," Nature **594**, 369–373 (2021).
 - ¹⁴⁰A. P. Vepsäläinen, A. H. Karamlou, J. L. Orrell, A. S. Dogra, B. Loer, F. Vasconcelos, D. K. Kim, A. J. Melville, B. M. Niedzielski, J. L. Yoder, S. Gustavsson, J. A. Formaggio, B. A. VanDevender, and W. D. Oliver, "Impact of ionizing radiation on superconducting qubit coherence," Nature **584**, 551–556 (2020).
 - ¹⁴¹L. Cardani, F. Valenti, N. Casali, G. Catelani, T. Charpentier, N. Clemenza, I. Colantoni, A. Cruciani, G. D'Imperio, L. Gironi, L. Grünhaupt, D. Gusenkova, F. Henriques, M. Lagoin, M. Martinez, G. Pettinari, C. Rusconi, O. Sander, C. Tomei, A. V. Ustinov, M. Weber, W. Wernsdorfer, M. Vignati, S. Pirro, and I. M. Pop, "Reducing the impact of radioactivity on quantum circuits in a deep-underground facility," Nature Communications **12**, 2733 (2021).
 - ¹⁴²B. K. Cooper, *Multi-junction effects in DC SQUID phase qubits*, Ph.D. thesis, University of Maryland (2013).
 - ¹⁴³S. M. Anton, J. S. Birenbaum, S. R. O'Kelley, V. Bolkhovskiy, D. A. Braje, G. Fitch, M. Neeley, G. C. Hilton, H.-M. Cho, K. D. Irwin, F. C. Wellstood, W. D. Oliver, A. Shnirman, and J. Clarke, "Magnetic flux noise in dc squids: Temperature and geometry dependence," Phys. Rev. Lett. **110**, 147002 (2013).
 - ¹⁴⁴S. L. Sendelbach, *Investigations of 1/f flux noise in superconducting quantum circuits*, Ph.D. thesis, University of Wisconsin–Madison (2013).
 - ¹⁴⁵D.-W. S. Inc., "The d-wave 2000q™ quantum computer technology overview," Overview.
 - ¹⁴⁶Y. Tabuchi, S. Ishino, A. Noguchi, T. Ishikawa, R. Yamazaki, K. Usami, and Y. Nakamura, "Quantum magnonics: The magnon meets the superconducting qubit," Comptes Rendus. Physique **17**, 729–739 (2016).
 - ¹⁴⁷J. S. Kelly, *Fault-tolerant superconducting qubits*, Ph.D. thesis, University of California in Santa Barbara (2015).
 - ¹⁴⁸M. Mirhosseini, E. Kim, X. Zhang, A. Sipahigil, P. B. Dieterle, A. J. Keller, A. Asenjo-Garcia, D. E. Chang, and O. Painter, "Cavity quantum electrodynamics with atom-like mirrors," Nature **569**, 692–697 (2019).
 - ¹⁴⁹Y. Sung, A. Vepsäläinen, J. Braumüller, F. Yan, J. I.-J. Wang, M. Kjaergaard, R. Winik, P. Krantz, A. Bengtsson, A. J. Melville, B. M. Niedzielski, M. E. Schwartz, D. K. Kim, J. L. Yoder, T. P. Orlando, S. Gustavsson, and W. D. Oliver, "Multi-level quantum noise spectroscopy," Nature Communications **12**, 967 (2021).
 - ¹⁵⁰A. Vidiorskiy, V. Koshelets, L. Filippenko, S. Shitov, and A. Ustinov, "Compacted tunable split-ring resonators," Applied Physics Letters **103**, 162602 (2013).
 - ¹⁵¹X. Li, Y. Zhang, C. Yang, Z. Li, J. Wang, T. Su, M. Chen, Y. Li, C. Li, Z. Mi, et al., "Vacuum-gap transmon qubits realized using flip-chip technology," Applied Physics Letters **119**, 184003 (2021).
 - ¹⁵²M. Pierre, I.-M. Svensson, S. R. Sathyamoorthy, G. Johansson, and P. Delsing, "Storage and on-demand release of microwaves using superconducting resonators with tunable coupling," APPLIED PHYSICS LETTERS **104**, 232604 (2014).
 - ¹⁵³A. Bengtsson, P. Vikstål, C. Warren, M. Svensson, X. Gu, A. F. Kockum, P. Krantz, C. Krizan, D. Shiri, I.-M. Svensson, G. Tancredi, G. Johansson, P. Delsing, G. Ferrini, and J. Bylander, "Improved success probability with greater circuit depth for the quantum approximate optimization algorithm," Phys. Rev. Appl. **14**, 034010 (2020).
 - ¹⁵⁴I. Wisby, *Hybrid rare-earth ion superconductor systems for quantum information processing*, Ph.D. thesis, Royal Holloway University of London (2017).
 - ¹⁵⁵Y. Wang, F. Luo, W. Zhou, and D. Zhu, "Dielectric and electromagnetic wave absorbing properties of tic/epoxy composites in the ghz range," Ce-

- ramics International **40**, 10749–10754 (2014).
- ¹⁵⁶J.-H. Yeh, Y. Huang, R. Zhang, S. Premaratne, J. LeFebvre, F. C. Wellstood, and B. S. Palmer, “Hot electron heatsinks for microwave attenuators below 100mK,” *Applied Physics Letters* **114**, 152602 (2019), https://pubs.aip.org/aip/apl/article-pdf/doi/10.1063/1.5097369/14524147/152602_1_online.pdf.
 - ¹⁵⁷D. T. Sank, *Fast, Accurate State Measurement in Superconducting Qubits*, Ph.D. thesis, University of California in Santa Barbara (2014).
 - ¹⁵⁸A. Schneider, T. Wolz, M. Pfirrmann, M. Spiecker, H. Rotzinger, A. V. Ustinov, and M. Weides, “Transmon qubit in a magnetic field: Evolution of coherence and transition frequency,” *Phys. Rev. Res.* **1**, 023003 (2019).
 - ¹⁵⁹D. Tan, S. J. Weber, I. Siddiqi, K. Mølmer, and K. W. Murch, “Prediction and retrodiction for a continuously monitored superconducting qubit,” *Phys. Rev. Lett.* **114**, 090403 (2015).
 - ¹⁶⁰A. I. Ivanov, V. I. Polozov, V. V. Echeistov, A. A. Samoylov, E. I. Mal'evannaya, A. R. Matanin, N. S. Smirnov, and I. A. Rodionov, “Robust cryogenic matched low-pass coaxial filters for quantum computing applications,” *Applied Physics Letters* **123**, 204001 (2023).
 - ¹⁶¹J. I. Colless, V. V. Ramasesh, D. Dahlen, M. S. Blok, M. E. Kimchi-Schwartz, J. R. McClean, J. Carter, W. A. de Jong, and I. Siddiqi, “Computation of molecular spectra on a quantum processor with an error-resilient algorithm,” *Phys. Rev. X* **8**, 011021 (2018).
 - ¹⁶²A. Opremcak, C. H. Liu, C. Wilen, K. Okubo, B. G. Christensen, D. Sank, T. C. White, A. Vainsencher, M. Giustina, A. Megrant, B. Burkett, B. L. T. Plourde, and R. McDermott, “High-fidelity measurement of a superconducting qubit using an on-chip microwave photon counter,” *Phys. Rev. X* **11**, 011027 (2021).
 - ¹⁶³L. Grünhaupt, M. Spiecker, D. Gusenkova, N. Maleeva, S. T. Skacel, I. Takmakov, F. Valenti, P. Winkel, H. Rotzinger, W. Wernsdorfer, A. V. Ustinov, and I. M. Pop, “Granular aluminium as a superconducting material for high-impedance quantum circuits,” *Nature Materials* **18**, 816–819 (2019).
 - ¹⁶⁴C. K. Andersen, A. Remm, S. Lazar, S. Krinner, J. Heinsoo, J.-C. Besse, M. Gabureac, A. Wallraff, and C. Eichler, “Entanglement stabilization using ancilla-based parity detection and real-time feedback in superconducting circuits,” *npj Quantum Information* **5**, 69 (2019).
 - ¹⁶⁵E. Leonard, M. A. Beck, J. Nelson, B. Christensen, T. Thorbeck, C. Howington, A. Opremcak, I. Pechenezhskiy, K. Dodge, N. Dupuis, M. Hutchings, J. Ku, F. Schlenker, J. Suttle, C. Wilen, S. Zhu, M. Vavilov, B. Plourde, and R. McDermott, “Digital coherent control of a superconducting qubit,” *Phys. Rev. Appl.* **11**, 014009 (2019).
 - ¹⁶⁶C. Song, T. W. Heitmann, M. P. DeFeo, K. Yu, R. McDermott, M. Neeley, J. M. Martinis, and B. L. T. Plourde, “Microwave response of vortices in superconducting thin films of Re and Al,” *Phys. Rev. B* **79**, 174512 (2009).
 - ¹⁶⁷A. Alexander, C. G. Weddle, and C. J. K. Richardson, “Power and temperature dependent model for high q superconductors,” (2025), [arXiv:2205.06291 \[quant-ph\]](https://arxiv.org/abs/2205.06291).
 - ¹⁶⁸J. Aumentado, M. W. Keller, J. M. Martinis, and M. H. Devoret, “Nonequilibrium quasiparticles and $2e$ periodicity in single-cooper-pair transistors,” *Phys. Rev. Lett.* **92**, 066802 (2004).
 - ¹⁶⁹M. D. Shaw, R. M. Lutchyn, P. Delsing, and P. M. Echternach, “Kinetics of nonequilibrium quasiparticle tunneling in superconducting charge qubits,” *Phys. Rev. B* **78**, 024503 (2008).
 - ¹⁷⁰U. Vool, I. M. Pop, K. Sliwa, B. Abdo, C. Wang, T. Brecht, Y. Y. Gao, S. Shankar, M. Hatridge, G. Catelani, M. Mirrahimi, L. Frunzio, R. J. Schoelkopf, L. I. Glazman, and M. H. Devoret, “Non-poissonian quantum jumps of a fluxonium qubit due to quasiparticle excitations,” *Phys. Rev. Lett.* **113**, 247001 (2014).
 - ¹⁷¹J. Wenner, Y. Yin, E. Lucero, R. Barends, Y. Chen, B. Chiaro, J. Kelly, M. Lenander, M. Mariantoni, A. Megrant, C. Neill, P. J. J. O'Malley, D. Sank, A. Vainsencher, H. Wang, T. C. White, A. N. Cleland, and J. M. Martinis, “Excitation of superconducting qubits from hot nonequilibrium quasiparticles,” *Phys. Rev. Lett.* **110**, 150502 (2013).
 - ¹⁷²J. M. Kitzman, J. R. Lane, T. Stefanski, N. R. Beysengulov, D. Tan, K. W. Murch, and J. Pollanen, “Vantablack shielding of superconducting qubit systems,” *Journal of Low Temperature Physics* **208**, 467–474 (2022).
 - ¹⁷³D. Ristè, C. C. Bultink, M. J. Tiggelman, R. N. Schouten, K. W. Lehnert, and L. DiCarlo, “Millisecond charge-parity fluctuations and induced decoherence in a superconducting transmon qubit,” *Nature Communications* **4**, 1913 (2013).
 - ¹⁷⁴R. Gordon, C. Murray, C. Kurter, M. Sandberg, S. Hall, K. Balakrishnan, R. Shelby, B. Wacaser, A. Stabile, J. Sleight, *et al.*, “Environmental radiation impact on lifetimes and quasiparticle tunneling rates of fixed-frequency transmon qubits,” *Applied Physics Letters* **120**, 074002 (2022).
 - ¹⁷⁵T. Connolly, P. D. Kurilovich, S. Diamond, H. Nho, C. G. L. Böttcher, L. I. Glazman, V. Fatemi, and M. H. Devoret, “Coexistence of nonequilibrium density and equilibrium energy distribution of quasiparticles in a superconducting qubit,” *Phys. Rev. Lett.* **132**, 217001 (2024).
 - ¹⁷⁶J. Kawai, M. Miyamoto, M. Kawabata, M. Nosé, Y. Haruta, and G. Uehara, “Characterization and demonstration results of a squid magnetometer system developed for geomagnetic field measurements,” *Superconductor Science and Technology* **30**, 084002 (2017).
 - ¹⁷⁷M. Schmelz, V. Zakosarenko, A. Chwala, T. Schönau, R. Stolz, S. Anders, S. Linzen, and H.-G. Meyer, “Thin-film-based ultralow noise squid magnetometer,” *IEEE Transactions on Applied Superconductivity* **26**, 1–5 (2016).
 - ¹⁷⁸J. Braumüller, L. Ding, A. P. Vepsäläinen, Y. Sung, M. Kjaergaard, T. Menke, R. Winik, D. Kim, B. M. Niedzielski, A. Melville, J. L. Yoder, C. F. Hirjibehedin, T. P. Orlando, S. Gustavsson, and W. D. Oliver, “Characterizing and optimizing qubit coherence based on squid geometry,” *Phys. Rev. Appl.* **13**, 054079 (2020).